FORMULATION OF A BEAM FINITE ELEMENT FOR MICRO BEAMS

A THESIS SUBMITTED TO
THE GRADUATE SCHOOL OF NATURAL AND APPLIED SCIENCES
OF
MIDDLE EAST TECHNICAL UNIVERSITY

BY

YÜCEL PEHLİVANOĞLU

IN PARTIAL FULFILLMENT OF THE REQUIREMENTS
FOR
THE DEGREE OF MASTER OF SCIENCE
IN
MECHANICAL ENGINEERING

MARCH 2018

Approval of Thesis:

FORMULATION OF A BEAM FINITE ELEMENT FOR MICRO BEAMS

Submitted by **YÜCEL PEHLİVANOĞLU** in partial fulfillment of the requirements for the degree of **Master of Science in Mechanical Engineering Department, Middle East Technical University** by,

Prof. Dr. Halil Kalıpçılar
Dean, Graduate School of **Natural and Applied Sciences** _____

Prof. Dr. M. A. Sahir Arıkan
Head of Department, **Mechanical Engineering** _____

Prof. Dr. F. Suat Kadıoğlu
Supervisor, **Mechanical Engineering Dept., METU** _____

Examining Committee Members:

Prof. Dr. Metin Akkök
Mechanical Engineering Dept., METU _____

Prof. Dr. F. Suat Kadıoğlu
Mechanical Engineering Dept., METU _____

Prof. Dr. Suha Oral
Mechanical Engineering Dept., METU _____

Asst. Prof. Dr. Hüsnü Dal
Mechanical Engineering Dept., METU _____

Asst. Prof. Dr. Barış Sabuncuoğlu
Mechanical Engineering Dept., Hacettepe University _____

Date: 12.03.2018

I hereby declare that all information in this document has been obtained and presented in accordance with academic rules and ethical conduct. I also declare that, as required by these rules and conduct, I have fully cited and referenced all material and results that are not original to this work.

Name, Last name: Yücel Pehlivanoğlu

Signature:

ABSTRACT

FORMULATION OF A BEAM FINITE ELEMENT FOR MICRO BEAMS

Pehlivanoğlu, Yücel
M.S., Department of Mechanical Engineering
Supervisor: Prof. Dr. F. Suat Kadıoğlu

March 2018, 117 pages

This study presents an Euler Bernoulli type micro-beam finite element for analyzing the size-dependent static and dynamic behavior of micro beams. The new element is based on Modified Couple Stress Theory (MCST). The governing equations of motion and the boundary conditions for the beam are derived and the conventional Galerkin technique is employed to formulate the finite element. The new element can be reduced to Classical Euler-Bernoulli beam element if the size-effect parameter in the element matrices is taken as zero. Using this finite element, static and free vibration analyses are carried out for different boundary conditions. The results are compared with analytical, numerical and similar finite element method based results in the literature and it is found that they are in good agreement. Two case studies are done to demonstrate possible uses of this beam finite element. One of the case studies pertains to the calculation of mesh stiffness of micro gears. This case study shows that there is a strong size effect for the mesh stiffness.

Keywords: Modified couple stress theory, micro-beams, mesh stiffness

ÖZ

MİKRO KİRİŞLER İÇİN KİRİŞ SONLU ELEMAN FORMÜLASYONU

Pehlivanoğlu, Yücel
M.S., Makine Mühendisliği Bölümü
Tez Yöneticisi: Prof. Dr. F. Suat Kadıoğlu

Mart 2018, 117 sayfa

Bu çalışmada, mikro kirişlerin, boyuta bağlı statik ve dinamik davranışlarını analiz etmek için, Euler-Bernoulli kiriş tipinde bir mikro kiriş sonlu elemanı elde edilmiştir. Bu yeni eleman modifiye edilmiş kuvvet çifti gerilmesi teorisi üzerine temellenmiştir. Kiriş için denklemler ve sınır şartları türetilmiş olup konvansiyonel Galerkin Tekniği kullanılarak sonlu eleman formüle edilmiştir. Eleman matrisleri içerisindeki boyut etkisi parametresi sıfır olarak alınırsa, bu yeni model, klasik Euler-Bernoulli kiriş elemanına indirgenebilir. Bu sonlu eleman kullanılarak, farklı sınır şartları için statik ve serbest titreşim analizleri yapılmıştır. Sonuçlar, literatürdeki analitik, numerik ve benzer sonlu eleman temelli çalışmalardan elde edilen sonuçlar ile kıyaslamış olup oldukça iyi örtüşmektedir. Bu elamanın olası kullanım alanlarını göstermek için iki özel durum incelemesi yapılmıştır. Bunlardan biri mikro dişli çarklar için diş direngenliğinin hesaplanmasıdır. Bu incelemeden elde edilen sonuçlar boyutun diş direngenliği üzerinde kuvvetli bir etkisi olduğunu göstermektedir.

Anahtar Kelimeler: Modifiye edilmiş kuvvet çifti gerilmesi teorisi, mikro kirişler, diş direngenliği

To My Family

ACKNOWLEDGMENTS

First of all, I am deeply grateful to my supervisor Prof. Dr. F. Suat Kadıoğlu for his guidance and support from the beginning to the end of this study.

I also thank examining committee members, Prof. Dr. Suha Oral, Prof. Dr. Metin Akkök, Dr. Hüsnü Dal, Dr. Barış Sabuncuoğlu for their valuable comments and contributions.

I would like to express my thanks to dear friends in TAI for their technical support throughout the thesis, especially to Mustafa Özgür Aydoğan and Mahir Gökhan Orak. In addition, for his guidance and kind leadership, I am deeply grateful to Dr. Zihni Burçay Sarıbay.

I would like to thank my parents, Mükremin Pehlivanoğlu and Aysel Pehlivanoğlu for their unfailing support and continuous encouragement through all my life. This accomplishment would not have been possible without them.

I also would like to thank my sweet sister Cansu Pehlivanoğlu for her selfless love and being my sister.

I would like to convey my deepest thanks to my lovely wife, Şule Pehlivanoğlu, whose understanding and love gave me the motivation to pass this challenging period of my life.

Finally, I would like to express my thanks to my little daughter, Aylin, for her patience when I was studying instead of playing together.

TABLE OF CONTENTS

LIST OF TABLES

TABLES

LIST OF FIGURES

FIGURES

LIST OF SYMBOLS

σ	Stress Tensor
ε	Strain tensor
m	Couple stress tensor
X	Curvature Tensor
θ	Rotation tensor
u	Displacement in *x* direction
v	Displacement in y direction
w	Displacement in z direction
ψ	Rotation Angle
h	Height of beam
b	Width of beam
A	Area of beam
m	mass of beam
L	Length of beam
λ	Lame's constant
l	material length scale parameter
E	Young's Modulus
μ	Shear Modulus
ρ	Density
ϑ	Poisson's ratio
I	Second moment of Inertia
F	Distributed force per unit length along transverse directions
G	Distributed force per unit length along axial directions

M	Bending moment
V	Shear force
N	Axial force
$Q's$	Generalized forces
X	Weight Function
$\boldsymbol{K}$	Stiffness Matrix
$\boldsymbol{M_t}$	Translational Mass Matrix
$\boldsymbol{M_\theta}$	Rotational Mass Matrix
$\boldsymbol{M}$	Total Mass Matrix
$\boldsymbol{F}$	Force Vector
α	Instantaneous pressure angle

CHAPTER 1

INTRODUCTION

1.1 Introduction

In recent years, developments in MEMS and nanotechnology attracted a great interest on the study of the mechanical behavior of extremely small beam like structures. The usage areas of micro and nano beam structures are rapidly increasing due to their advantages [1] such as: smaller package size, lower cost, lighter weight, less power consumption, wider operating temperature range etc. Another advantage is the increasing strength of the material in micro scale. For example, in the micro-torsion experiment of thin copper wires in 1994, Fleck et al. [2] observed that the torsional hardening increase by a factor of 3 if the wire diameter is decreased from 170 to 12 μm**.** Due to those advantages, micro beams are becoming more and more popular and they are used in many different areas. A micro beam can be used, for instance, as a sensor in active suspension systems in automotive industry or for military purposes such as in a tank's gyroscope and in some other military equipment. In medicine, micro beams are used in bio-mems [1]. For example, micro beam structures exist in devices used for drug resistance detection [3]**.**

An understanding of the behavior of micro and nanostructures used in different applications such as engineering, medicine etc. is very important. In order to have advancements in the area of MEMS and nanotechnology, it is very important to accurately predict the mechanical behavior of such structures, under different loading and boundary conditions. Commercial FEA software programs provide many types of beam elements with various features. These elements could be used to analyze macroscopic structures made up of beams. However, when one considers extremely

small beam structures, size effects become important. There are a number of theoretical and analytical approaches to deal with beams and plates at micro-scale such as strain gradient elasticity theory or modified couple stress theory. Isolated micro beams can be analyzed by using various analytical or numerical methods based on these theories. However, when a number of micro-beams are joined to form a micro-structure such as a micro frame under various boundary conditions, obtaining analytic solutions could become very cumbersome. To solve such problems numerically by using the desired micro-scale theory, finite elements appropriate for the theory used should be developed, because such elements with the required features are not readily available in the commercial FEM software.

According to classical elasticity, the material is formed by a particular atomistic system, such as a crystal lattice. The elastic body could be small or large but the internal structure at every point of the body would be the same, only the expanse of the same structure becomes larger upon increasing the sample size. This view is correct for some materials such as diamond. That is why classical continuum theory is inherently size dependent. The microstructural features that may exist above atomistic but below macroscopic scale are not taken into consideration. However in reality, for many materials, such as polycrystalline solids, there are discrete microstructural features such as grain boundaries, dislocations etc. at intermediate scales. Although this is contrary to the assumption of classical theory, when the size of the elastic body is sufficiently large compared to the microstructural features, the material properties average out and classical elasticity could still be used successfully in many applications. However when the size of the body becomes comparable to the size of microstructural features, deviations from classical theory start manifesting themselves. Moreover, there are different types of physical mechanisms such as surface energy effects and nonlocal interactions [4] which lead to nonlocal stress strain relationships at microscopic scales, which are again not considered by classical continuum theories. All those can be investigated under the term “size effect”. Size effect is the reason why classical

continuum theories fail to accurately predict the mechanical behavior of microstructures. As the dimensions of structures become smaller and smaller such that any dimension is comparable with materials' micro structure, size effects are observed. In order to capture the size effect, the constitutive equations should contain material length scale parameters. This motivated the development of beam models in which higher-order (non-local) continuum theories that contain additional material parameters are used.

The objective of this thesis is to develop a micro-beam finite element and to develop a Finite Element Method code based on it, which could be used to analyze micro mechanical systems made of beams. In order to derive the equilibrium equations of micro-beams, Euler-Bernoulli beam theory, along with Modified Couple Stress Theory (MCST) is used. Using variational formulation governing equations are derived and by using a weighted residual technique finite element matrices are obtained. Verification studies are done by using developed FEM code and the derived element. Numerical results are obtained. These results are compared with published work to verify their accuracy and reliability. Then two case studies are done and their results are presented.

1.2 Literature Survey

In recent decades, the size dependence of load-deformation behavior in micro scale is experimentally shown for some metals and polymers. The very early experiments were performed by Fleck et al. [2] to determine length scale parameter**.** They performed torsional experiments on copper wires. The study showed that in order to have the same strain values, the thin wires (∼15 μm) required significantly higher torques than thicker wires. Length scale effects are further investigated by utilizing indentation experiments (Atkinson [5], Ma & Clarke [6], Poole et al. [7], Begley & Hutchinson [8], Shu & Fleck [9], Nix & Gao [10], McElhaney et al. [11], Lim & Chaudhri [12], Swadener [13], Tao et al. [14], Huang et al. [15], Qu et al. [16], Harsano et al. [17]), fracture experiment (Wei & Hutchinson [18]) and micro-bending experiments (Stölken & Evans [19], Shrotriya et al. [20], Wang et al. [21]).

Although there are many experimental approaches to understand the size effect, doing experiments is still a challenge to study the mechanics of materials in micro and nanoscale because of the difficulties encountered. Therefore, nowadays, analytical and numerical methods based on higher order (size dependent) continuum mechanics theories are preferred to study the behavior of micro and nanostructures. Due to the fact that beam models based on classical elasticity fail to describe the size effects, new beam models in which higher-order continuum theories having additional material parameters are being used.

In 1960s, Mindlin & Tiersten [22], Mindlin [23], [24] and Toupin [25] introduced the couple stress elasticity theory by using couple per unit area which acts across a surface within a material volume or on its boundary in addition to the usual force per unit area. In this theory, an additional modulus of elasticity related with bending and twisting with the dimension of force appears. The square root of the ratio of this modulus to the usual shear modulus has the dimension of length. This new parameter, called length scale

parameter, is also a material property. There are two higher-order material length scale parameters, in this theory, in addition to the two classical Lame constants. Then classical couple stress theory is extended by Fleck & Hutchinson [26]–[28]. In this theory, second order deformation gradient is decomposed into two independent parts, namely stretch gradient and rotation gradient. Three more additional higher order length scale parameters are added for stretch and rotation gradient theories.

In 2002, in order to reduce the difficulties encountered to determine length scale parameters of materials by experiments, Yang et al. [29] presented the modified couple stress theory (MCST). By adding moment of couples to the equilibrium equations, the couple stress tensor is restricted to be symmetric and deformation energy becomes independent of antisymmetric part of the curvature tensor. This reduces the requirement of length scale parameter in the constitutive equations form two to one. By analyzing the torsion of a cylindrical bar and bending of a flat plate, new modification is investigated.

In 2003, Lam et al. [30] considered the second order deformation gradient together with the classical symmetric strain tensor and generated the modified version of strain gradient theory (SGT) proposed by Fleck & Hutchinson [26]–[28] before. In this paper, ‘‘strain gradient’’ wording is used to define the modified version of the theory. In this theory, three independent higher-order material length scale parameters for isotropic linear elastic materials are introduced. A simple cantilever beam subjected to bending is used to investigate the difference between classical and strain gradient elastic theories. It is shown that the higher order theory accurately demonstrates the behavior of micro - sized epoxy beams in an experiment.

Another widely used size-dependent continuum theory is nonlocal elasticity theory which is proposed by Eringen [31]**.** This theory yields results dependent on the size of the body because it considers long range inter-atomic interactions. It assumes that stress at a point depends on not only strain at that point but also strain at every point in the

body. In the nonlocal theory of Eringen, one length scale parameter is used to capture the size effect.

The number of lame constants and higher order parameters of each corresponding theory are given in Table 1.

Table 1. Number of parameters for different theories

	Lame constants	**Higher order parameter**	**TOTAL**
Classical Elasticity	2	0	2
Mindlin's Couple Stress Theory	2	2	4
Fleck's Strain Gradient Theory	2	5	7
Yang's Modified Couple Stress Theory (MCST)	2	1	3
Lam's Strain Gradient Theory (SGT)	2	3	5
Eringen's Non-Local Theory	2	1	3

Among these theories, Eringen's Non-local Theory, Strain Gradient Elasticity theory and Modified Couple stress theory stand out as the three most commonly used theories in the recent literature.

In order to have a useful model of the static and dynamic responses of micro and nano beams used in structures, the size dependent continuum theories are combined with appropriate beam theories. . In the following part of this literature survey, the three most commonly used continuum theories are considered and studies are categorized according to the size dependent continuum theory that was adopted. In some of the studies, more

than one continuum theory is used and the results obtained through different theories are compared.

1.2.1 Studies based on Eringen's Non-local Elasticity Theory

In some studies, homogenous beams are investigated by using classical Euler-Bernoulli beam theory together with Eringen's non-local theory in differential form. Bending, buckling and vibration characteristics of those beams are investigated under various boundary and loading conditions. The obtained governing equations are solved with finite element approach in some of the studies, such as Phadikar & Pradhan [32], Eltaher et al. [33], Mahmoud et al. [34]. Moreover, Eltaher et al. [35] studied static loading and stability of functionally graded nanobeams in a similar manner. In the work of Reddy & El-Borgi [36], both Euler-Bernoulli and Timoshenko beams are used which account for moderate rotations. Non-linear finite element models are developed. Reddy et al. [37], further investigated the nonlinear finite element model for functionally graded beams. Pradhan [38] considered both Timoshenko and Euler-Bernoulli beams and used nonlocal elasticity to understand the behavior of Carbon nano-tubes (CNTs) with different boundary conditions. Pisano et al. [39] extended the work done with beams and analyzed nonlocal 2D problems. Natarajan et al. [40] studied vibrational behavior of functionally graded nano plates including size effect.

There are also researchers who used differential quadrature method. Civalek & Demir [41] utilized Euler-Bernoulli beam theory to understand the bending behavior of microtubules. Static analysis is carried out using the differential quadrature method. In the works of Nejad & Hadi [42], Nejad et al. [43], Nejad & Hadi [44] nonlocal vibrations, buckling and bending are investigated for bi-directional functionally graded Euler-Bernouli nanobeams with generalized differential quadrature method. Ghadiri & Shafiei [45] studied nonlinear bending vibration of an Euler-Bernoulli beam with von Karman

geometric nonlinearity. Shafiei et al. [46] studied the nonlinear vibration analysis of axially functionally graded Euler-Bernoulli nano beams. Solution is obtained by using homotopy perturbation method together with generalized differential quadrature method. By using differential quadrature method and Eringen's nonlocal elasticity, some researchers also performed 2D plate analyses [47],[48].

There are also studies in the literature where Eringen's nonlocal theory is used and analytical solutions are obtained. Reddy [49] and Aydogdu [50] derived equations of motions for different beam theories based on Eringen's nonlocal theory and solved them analytically to investigate the bending, buckling and vibration behaviors of simply supported beams. In another study, based on nonlocal elasticity theory, longitudinal frequency of a cracked nanobeam is considered analytically by Hsu et al. [51]. They investigated the effects of the crack parameter, crack location and nonlocal parameter on frequency of a cracked nanobeam. Murmu & Adhikari [52] studied coupled nanobeam system under pre-compressive stress condition by using Eringen's nonlocal elasticity theory and solved this problem analytically. Şimşek & Yurtçu [53] studied bending and buckling behavior of both Timoshenko and Euler-Bernoulli beams which are made of functionally graded materials. In an another set of studies, Uymaz [54] and Rahmani & Pedram [55] studied vibration behaviour and Nazemnezhad & Hosseini-Hashemi [56] studied nonlinear vibration behaviour of functionally graded nanobeams analytically.

Recently, some researches revealed that Eringen's nonlocal elasticity theory in differential form has some inconsistencies for some type of problems. Therefore, Tuna & Kırca [57] and Fernandez et al. [58] investigated static bending of Timoshenko and Euler-Bernoulli beam models analytically by using integral form of Eringen's nonlocal theory. In another study, Salehipour et al. [59] introduced an imaginary nonlocal stress tensor to the Eringen's nonlocal theory to obtain more accurate results for functionally graded plates. By using this new modified theory, functionally graded plates are investigated. Khodabakhshi & Reddy [60] proposed a new integro-differential nonlocal

elasticity theory to eliminate the inconsistencies in the differential form of Eringen's theory. Finite element formulation is obtained and Euler-Bernoulli beam is used to investigate the bending behavior.

1.2.2 Studies based on Strain Gradient Elasticity Theory

In the literature, there are also studies utilizing the strain gradient theory (SGT). Most of them contain analytical solutions to beam problems. Kong et al. [61] studied static and dynamic response of Euler-Bernoulli beams on the basis of SGT and obtained analytical solutions. Timoshenko beam model is considered together with SGT by Wang et al. [62] and bending and vibration analysis of a simply supported beam are investigated analytically. Kahrobaiyan et al. [63] developed a nonlinear size-dependent Euler-Bernoulli beam theory based on SGT. They consider mid-plane stretching as the source of nonlinearity in the beam behavior and analytical solutions are derived. This work is extended in Kahrobaiyan et al. [64] by avoiding the assumption of constant length scale parameter through the thickness. They introduced equivalent length scale parameter for functionally graded micro beams. In another research, utilizing SGT and Euler-Bernoulli beam, size effect on buckling of microtubules was studied by Akgöz & Civalek [65]. Akgöz & Civalek [66], [67] also studied bending and buckling behaviors of both uniform and functionally graded beam models.

Aghazadeh [68], considered functionally graded Timoshenko beams based on strain gradient theory. Differential quadrature method is utilized for the solution. In this work, static and free vibration analysis are done using the newly developed method.

Recently, there are works that utilize SGT where the finite element method is adopted as the solution method. Zhang et al. [69] considered bending, free vibration and buckling behavior of a Timoshenko beam by using finite element method. Moreover, Hosseini &

Bahaadini [70] undertook stability analysis for cantilever micro-pipes conveying fluid using SGT. Finally, Dal [71] studied Euler-Bernoulli Gold-micro beams based on Strain Gradient theory by using Galerkin type finite element approach.

1.2.3 Studies based on Modified Couple Stress Theory

Modified couple stress theory is also used by many researchers to study the mechanics of micro and nano beams. There are numerous analytical studies. Park & Gao [72], Kong et al. [73] and Xia et al. [74] studied Euler Bernoulli beams based on MCST and obtained deflection, buckling behavior and natural frequencies of the beams. Park & Gao [75] derived the equilibrium equations and boundary conditions simultaneously by providing a variational formulation for MCST which completes the work of Yang et al. [29]. Asghari et al. [76] studied functionally graded materials and obtained static and vibration behavior of Euler Bernoulli beams based on MCST. In another work of Asghari et al. [77] size dependent Timoshenko beams made of FGM are investigated by using MCST. Reddy [78], investigated functionally graded beams based on MCST and Timoshenko beam theory. In this work, Reddy considers von-Karman nonlinearity and power law variation of FGM. Fu & Zhang [79] derived a Timoshenko beam model in order to capture the size effect on bending and buckling behavior of microtubules. In another study, Ma et al. [80] investigated Timoshenko beam theory based on MCST by considering Poisson effect, which is neglected in most of the studies, and they obtained bending and axial deformations of micro beams. Akgöz & Civalek [81] studied stability of axially loaded nano sized beams. Based on SGT, MCST and classical elasticity together with Euler-Bernoulli beam theory, authors derived the governing equations. In this work, the results for different theories are compared. Carbon nanotubes (CNTs) are also considered by some researchers based on MCST. In an analytical study of Akgöz et al. [82] stability analysis of CNTs using Euler-Bernoulli beam theory are investigated.

Fakhrabadi et al. [83] applied MCST to CNTs which are under step DC voltage and studied their vibration behavior. In the work of Şimşek [84], for an Euler-Bernoulli beam on a nonlinear elastic foundation, a nonlinear analysis is done by using MCST. Ghayesh & Farokhi [85] investigated chaotic motion of micro beam subjected to an axial load which is varying with time. Rahaeifard [86] studied the behavior of bilayer Euler-Bernoulli micro beam under thermal actuation. In another study, Sourki & Hoseini [87] investigated the free transverse vibration of an Euler-Bernoulli beam which is cracked. Mohammed-Abadi & Daneshmehr [88] considered buckling laminated composite Timoshenko and Euler-Bernoulli beams by using MCST. Recently, Thai et al. [89] investigated bending, buckling and free vibration of functionally graded sandwich Timoshenko micro beams. In this study, both homogenous core & functionally graded skin and homogenous skin & functionally graded core type sandwiches are considered. Ilkhani & Hosseini-Hashemi [90] studied free vibrations and stability of rotating Timoshenko and Euler-Bernoulli micro beams by considering effects of tangential load and Coriolis force. Şimşek & Reddy [91], studied static bending and free vibration of functionally graded micro beams based on a newly developed higher order beam theory and MCST. In this study, various higher order beam theories are used. Lately, analytical studies for plates are encountered in the literature. Lei et al. [92] studied functionally graded micro-plate model based on MCST. Similarly, in the study of Lou et al. [93], a unified higher order plate theory is used for functionally graded micro-plates. Taati [94] studied buckling and post buckling behavior of micro-plates for different boundary and loading conditions. Guo et al. [95] analytically investigated the size-dependent behavior of functionally graded anisotropic elastic composites based on MCST. Lou et al. [96] studied bending and free vibration behavior of functionally graded micro-plate on an elastic foundation. In this work, a nonlinear plate model is developed and this model is compared with the linear counterpart.

Some researchers used differential quadrature method to solve the governing equations, which are derived by using modified couple stress theory. In the work of Wang [97],

vibration analysis of fluid-conveying micro tubes is investigated. An analytical model is derived and differential quadrature method is used for discretization. Ke et al. [98] investigated the nonlinear free vibration of Timoshenko micro beams made of functionally graded materials. In different studies [99], [100], [101] conducted by Shafiei et al., transverse vibrations of rotary tapered axially functionally graded micro beams, nonlinear vibration behavior of imperfect uniform and non-uniform functionally graded micro beams, and nonlinear non-uniform axially functionally graded micro beams are investigated respectively. In these studies, authors utilized MCST, Euler-Bernoulli beam model and differential quadrature method. Muhammed-Abadi & Daneshmehr [102] considered buckling analysis for three different beam models: Euler-Bernoulli, Timoshenko and Reddy beam models. In the same study, analytical solutions are also employed for those three different beam theories and two solution types are compared. Akbarzadeh et al. [103] focused on the nonlinear post buckling behavior of functionally graded Nano beams for which general deformation beam theory and MCST are used . In this work, Young's modulus and material length scale parameter of beam are assumed to vary across thickness.

Recently, finite element solutions are used in a number of the studies, which are based on MCST. Arbind & Reddy [104] investigated nonlinear functionally graded Timoshenko and Euler-Bernoulli beams. Kahrobaiyan et al. [105], studied Timoshenko beam model utilizing finite element approach. Both stiffness and mass matrices are derived. Two case studies are carried out. The results are compared with those of both classical beam theories and experiments. Some of the results given in this study are used as benchmark results in this thesis. Dai & Wang [106] studied nonlinear dynamics of a micro cantilever beam. In different studies, Dehrouyeh-Semnani [107], Dehrouyeh-Semnani & Nikkhah-Bahrami [108] and Dehrouyeh-Semnani et al. [109] utilized MCST and finite element model to investigate behavior of micro-beams. They considered flap wise vibration frequency of rotating micro beams, shear deformation influence on static bending, buckling, free vibration behavior of micro beams and flexural frequency

characteristics of rotating micro cantilever beam due to vibration in the plane of rotating axis, respectively. In another work, Dehrouyeh-Semnani & Arian Bahrami [110] considered Timoshenko beam theory based on MCST. The equations are solved using finite element method by using elements having both 3-DOF (degree of freedom) and 2 –DOF at nodes. Recently, Reddy et al. [111], developed nonlinear finite element model for circular plates based on MCST.

Table 2 that summarizes the work in the literature is given below:

Table 2. Summary of literature survey according to the adopted method of solution, beam and continuum theories

Finite Element Solution Analytical Solution DQM Solution	Timoshenko Beam	Euler-Bernoulli Beam	Plate
Nonlocal elasticity of Eringen	Reddy 2007 [49] Aydogdu 2009 [50] Şimşek & Yurtçu 2014 [53] Uymaz 2013 [54] Rahmani & Pedram 2014 [55] Pradhan 2012 [38] Reddy & El-Borgi 2014 [36] Reddy et al. 2014 [37]	Hsu et al. 2011 [51] Murmu & Adhikari 2012 [52] Nazemnezhad & H.Hashemi 2012 [56] Tuna & Kırca 2016 [57] Fernandez et al. 2016 [58] Civalek & Demir 2011 [41] Nejad & Hadi 2016 [42] Nejad et al. 2016 [43] Nejad & Hadi 2016 [44] Ghadiri & Shafiei 2016 [45] Shafiei et al. 2016 [46] Phadikar & Pradhan 2010 [32] Eltaher et al. 2012 [33] Mahmoud et al. 2012 [34] Eltaher et al. 2013 [35] Khodabakhshi & Reddy 2015 [60]	Salehipour et al. 2015 [59] Daneshmehr et al. 2014 [47] Daneshmehr et al. 2015 [48] Pisano et al. 2009 [39] Natarajan et al. 2012 [40]
Modified Couple Stress Theory	Asghari et al. 2011 [77] Reddy 2011 [78] Fu & Zhang 2010 [79] Ma et al. 2008 [80] Abadi & Daneshmehr 2014 [88] Thai et al. 2015 [89] Ilkhani & H. Hashemi 2016 [90] Ke et al. 2012 [98] Abadi & Daneshmehr [102] Akbarzadeh et al. 2016 [103] Arbind & Reddy 2013 [104] Kahrobaiyan et al. 2014 [105] Dai & Wang 2015 [106] D.Semnani & N.Bahrami 2015 [108] D.Semnani et al. 2016 [109] D.Semnani & A.Bahrami 2015 [110]	Park & Gao 2006 [72] Kong et al. 2008 [73] Xia et al. 2010 [74] Park & Gao 2008 [75] Asghari et al. 2010 [76] Akgöz & Civalek 2011 [81] Akgöz et al. 2011 [82] Fakhrabadi et al. 2013 [83] Şimşek 2014 [84] Ghayesh & Farokhi 2015 [85] Rahaeifard 2016 [86] Sourki & Hoseini 2016 [87] Wang 2010 [97] Shafiei et al. 2016a [99] Shafiei et al. 2016b [100] Shafiei et al. 2016c [101] D.Semnani 2015 [107]	Lei et al. 2015 [92] Lou et al. 2015 [93] Taati et al. 2016 [94] Guo et al. 2016 [95] Lou et al. 2016 [96] Reddy et al. 2016 [111]
Strain Gradient Elasticity Theory	Wang et al. 2010 [62] Akgöz & Civalek 2014a [66] Akgöz & Civalek 2014b [67] Reza 2013 [68] Zhang et al. 2014 [69]	Kong et al. 2009 [61] Kahrobaiyan et al 2011 [63] Kahrobaiyan et al. 2012 [64] Akgöz & Civalek 2011 [65] Hosseini & Bahaadini 2016 [70] Dal 2017 [71]	

The literature survey presented above indicates that mechanical response of micro beams have been extensively studied within the past two decades. In order to show the differences between macro and micro scale behaviors of structures researches did analytical and numerical studies. Therefore, approaches of using higher order continuum theories together with different kind of beam theories become more and more popular. Most of the articles presented above show the difference between micro and macro scale behaviors of different kinds of beams either analytically or numerically. They are in very good agreement to represent the differences in micro scale. They not only show the difference but also specify at which scales the higher order continuum theories should be considered instead of classical ones.

Although, there are many studies in the literature about micro scale structure behaviors, especially in the last ten years, there are still topics need to be worked. For instance, there are numerous studies for micro beams. However, relatively few number of plate studies exist, especially plate theories using strain gradient elasticity theory. Moreover, there are only few material types whose length scale parameter values are determined by experiment. All studies focuses on those few materials. A set of experimental studies can be carried out to determine other kind of materials' length scale parameters that are used in micro scale structures. Furthermore, studies generally consider the solution of generalized beam theories, which is important. However, only a few of the studies specifically deals with the micro beam applications, instead of simple beams with various support conditions. It is considered that, literature have a place to expand towards application areas of micro beams.

1.3 Motivation and the Scope of the Study

Analytical and numerical studies to understand the size effect observed in the mechanical response of micro beams are commonly based on Eringen's non-local theory. Relatively

newer higher order theories, namely SGT and MCST, are also frequently used. Although there are many analytical studies utilizing SGT and MCST, numerical investigations where FEM was adopted, are relatively fewer. Hence numerical studies are still standing as an open topic. It is known that, although the analytical solutions could give the result directly for standalone beams under various boundary and loading conditions, when a number of micro-beams are joined to form a micro-structure, analytic solutions could become rather cumbersome. Currently, common commercial FEA software such as ANSYS®, ABAQUS® and COMSOL® do not offer beam, plate, or solid elements based on higher order continuum theories. Although some of the software programs have some special plugins or user defined interfaces to form stiffness matrices or mass matrices, there is still no single and powerful software for this kind of small-scale applications. It is therefore deemed worthwhile to formulate finite elements and implement them in codes to study the size effect for the mechanical response of micro scale structures.

In this thesis, Modified Couple Stress Theory (MCST) proposed by Yang et al. [29] is chosen as the higher order continuum theory. With regard to the related literature, it can be stated that, MCST simulates the behavior of micro structures quite satisfactorily. Although, it is a reduced form of Strain Gradient theory (SGT) proposed by Lam et al. [30], by comparing the studies in the literature, it can be inferred that MCST works almost as well as SGT. Moreover, the MCST requires only one length scale parameter whereas SGT which requires three length scale parameters. This property of MCST makes it "easy to apply" higher order continuum theory.

In this study, MCST is used along with Euler-Bernoulli beam theory to develop a beam finite element. MATLAB® is used to develop a finite element code capable of solving static problems and performing free vibration analysis. In order to verify the developed element and the code, a number of problems whose solutions are available in the literature are solved. The results are compared with both analytical and numerical

solutions. Moreover, two original case studies are carried out. In the first case study, a frame structure made-up of micro beams is considered. The static behavior under load and natural frequencies are investigated. In the second case study, mesh stiffness calculations of micro scale spur gear pairs are carried out.

1.4 Outline of the Thesis

In Chapter 2 (Formulation), by using Modified Couple Stress theory and Euler Bernoulli Beam Theory (EBT), governing equations and boundary conditions for transverse and axial directions are obtained by applying Hamilton's principle.

In Chapter 3 (Numerical Solution), obtained governing equations are considered for two special cases separately. These cases are static loading and free vibration. The equations are discretized for numerical solution by using classical Galerkin method. MATLAB® is used to obtain elemental stiffness and mass matrices, and nodal force vectors.

In Chapter 4 (Results), the obtained stiffness and mass matrices are compared with the studies in the literature. Several numerical results given in the literature are duplicated with the developed element and the code. After verification is completed, two original case studies are performed. The first case study is the static and dynamic behavior of a 2D frame. The second case study is the mesh stiffness calculation of micro spur gears.

In Chapter 5 (Conclusion and Future Work), conclusions are discussed and possible future works are suggested.

CHAPTER 2

FORMULATION

The strain energy of MCST is given in Yang et al [29] as

$$U = \frac{1}{2}\int \big(\sigma_{xx}\varepsilon_{xx} + \mathrm{m}_{xx}\chi_{xx} + \sigma_{yy}\varepsilon_{yy} + \mathrm{m}_{yy}\chi_{yy} + \sigma_{zz}\varepsilon_{zz} + \mathrm{m}_{zz}\chi_{zz} + \sigma_{xy}\varepsilon_{xy} + \mathrm{m}_{xy}\chi_{xy} + +\sigma_{yz}\varepsilon_{yz} + \mathrm{m}_{yz}\chi_{yz} + \sigma_{zx}\varepsilon_{zx} + \mathrm{m}_{zx}\chi_{zx}\big)dv, \tag{2.1}$$

where for isotropic case one can write

$$\sigma_{xx} = \lambda\varepsilon_{kk} + 2\mu\varepsilon_{xx,} \tag{2.2a}$$

$$\sigma_{yy} = \lambda\varepsilon_{kk} + 2\mu\varepsilon_{yy,} \tag{2.2b}$$

$$\sigma_{zz} = \lambda\varepsilon_{kk} + 2\mu\varepsilon_{zz}, \tag{2.2c}$$

$$\sigma_{xy} = 2\mu\varepsilon_{xy,} \tag{2.2d}$$

$$\sigma_{yz} = 2\mu\varepsilon_{yz}, \tag{2.2e}$$

$$\sigma_{zx} = 2\mu\varepsilon_{zx}, \tag{2.2f}$$

$$\varepsilon_{xx} = \frac{\partial u}{\partial x}, \tag{2.3a}$$

$$\varepsilon_{yy} = \frac{\partial v}{\partial x}, \tag{2.3b}$$

$$\varepsilon_{zz} = \frac{\partial w}{\partial x}, \tag{2.3c}$$

$$\varepsilon_{xy} = \varepsilon_{yx} = \frac{1}{2}\left(\frac{\partial u}{\partial y} + \frac{\partial v}{\partial x}\right), \tag{2.3d}$$

$$\varepsilon_{yz} = \varepsilon_{zy} = \frac{1}{2}\left(\frac{\partial v}{\partial z} + \frac{\partial w}{\partial y}\right), \tag{2.3e}$$

$$\varepsilon_{zx} = \varepsilon_{xz} = \frac{1}{2}\left(\frac{\partial u}{\partial z} + \frac{\partial w}{\partial x}\right), \tag{2.3f}$$

$$\varepsilon_{kk} = \varepsilon_{xx} + \varepsilon_{yy} + \varepsilon_{zz}, \tag{2.3g}$$

$$\mathrm{m}_{xx} = \beta\chi_{xx} = 2l^2\mu\chi_{xx}, \tag{2.4a}$$

$$\mathrm{m}_{yy} = \beta\chi_{yy} = 2l^2\mu\chi_{yy}, \tag{2.4b}$$

$$\mathrm{m}_{zz} = \beta\chi_{zz} = 2l^2\mu\chi_{yy}, \tag{2.4c}$$

$$\mathrm{m}_{xy} = \mathrm{m}_{yx} = \beta\chi_{xy} = 2l^2\mu\chi_{xy}, \tag{2.4d}$$

$$\mathrm{m}_{yz} = \mathrm{m}_{zy} = \beta\chi_{yz} = 2l^2\mu\chi_{yz}, \tag{2.4e}$$

$$\mathrm{m}_{zx} = \mathrm{m}_{xz} = \beta\chi_{xz} = 2l^2\mu\chi_{xz}, \tag{2.4f}$$

$$\theta_x = \theta_{zy} = \frac{1}{2}\left(\frac{\partial w}{\partial y} - \frac{\partial v}{\partial z}\right), \tag{2.5a}$$

$$\theta_y = \theta_{xz} = \frac{1}{2}\left(\frac{\partial u}{\partial z} - \frac{\partial w}{\partial x}\right), \tag{2.5b}$$

$$\theta_z = \theta_{yx} = \frac{1}{2}\left(\frac{\partial v}{\partial x} - \frac{\partial u}{\partial y}\right), \tag{2.5c}$$

$$X_{xx} = \frac{\partial \theta_x}{\partial x}, \tag{2.6a}$$

$$X_{yy} = \frac{\partial \theta_y}{\partial y}, \tag{2.6b}$$

$$X_{zz} = \frac{\partial \theta_z}{\partial z}, \tag{2.6c}$$

$$X_{xy} = X_{yx} = \frac{1}{2}\left(\frac{\partial \theta_x}{\partial y} + \frac{\partial \theta_y}{\partial x}\right), \tag{2.6d}$$

$$X_{yz} = X_{zy} = \frac{1}{2}\left(\frac{\partial \theta_y}{\partial z} + \frac{\partial \theta_z}{\partial y}\right), \tag{2.6e}$$

$$X_{zx} = X_{xz} = \frac{1}{2}\left(\frac{\partial \theta_x}{\partial z} + \frac{\partial \theta_z}{\partial x}\right), \tag{2.6f}$$

where

σ, Stress tensor

ε, Strain tensor

m, Couple stress tensor

X, Curvature Tensor

θ_x, θ_y , θ_z elements of rotation tensor

u,*v*,*w*, displacements in *x*,*y*,*z* directions

λ & μ Lame's constants

l, material length scale parameter.

For an Euler-Bernoulli beam, the displacement field is given as

$$u = u(x,t) + z\psi(x,t), \tag{2.7a}$$

$$v = 0, \tag{2.7b}$$

$$w = w(x,t), \tag{2.7c}$$

where u, v and w are the displacements along x,y and z axis respectively and ψ is the rotation angle resulting from the deflection of the beam. In the subsequent derivations reference [73] is followed

$$\psi(x,t) \approx -\frac{\partial w(x,t)}{\partial x}. \tag{2.8}$$

Using eqn.'s (2.3a), (2.7a) and (2.8) the only non-zero strain component is obtained as

$$\varepsilon_{xx} = \frac{\partial u(x,t)}{\partial x} - z\frac{\partial^2 w(x,t)}{\partial x^2}. \tag{2.9}$$

All other strain components are zero, i.e.

$$\varepsilon_{xy} = \varepsilon_{yz} = \varepsilon_{zx} = \varepsilon_{yy} = \varepsilon_{zz} = 0.$$

Moreover, from eqn. (2.8) and eqn. (2.5a), it follows that

$$\theta_y = -\frac{\partial w(x,t)}{\partial x}, \tag{2.10}$$
$$\theta_x = \theta_z = 0.$$

Then, if equation eqn. (2.10) is substituted into eqn. (2.6a)

$$\chi_{xy} = -\frac{1}{2}\frac{\partial^2 w(x,t)}{\partial x^2}. \tag{2.11}$$

All the other elements of curvature tensor are zero, i.e.

$$\chi_{yz} = \chi_{zx} = \chi_{xx} = \chi_{yy} = \chi_{zz} = 0.$$

Schematic diagram of Cartesian coordinate system for Euler-Bernoulli beam is given in Figure 1.

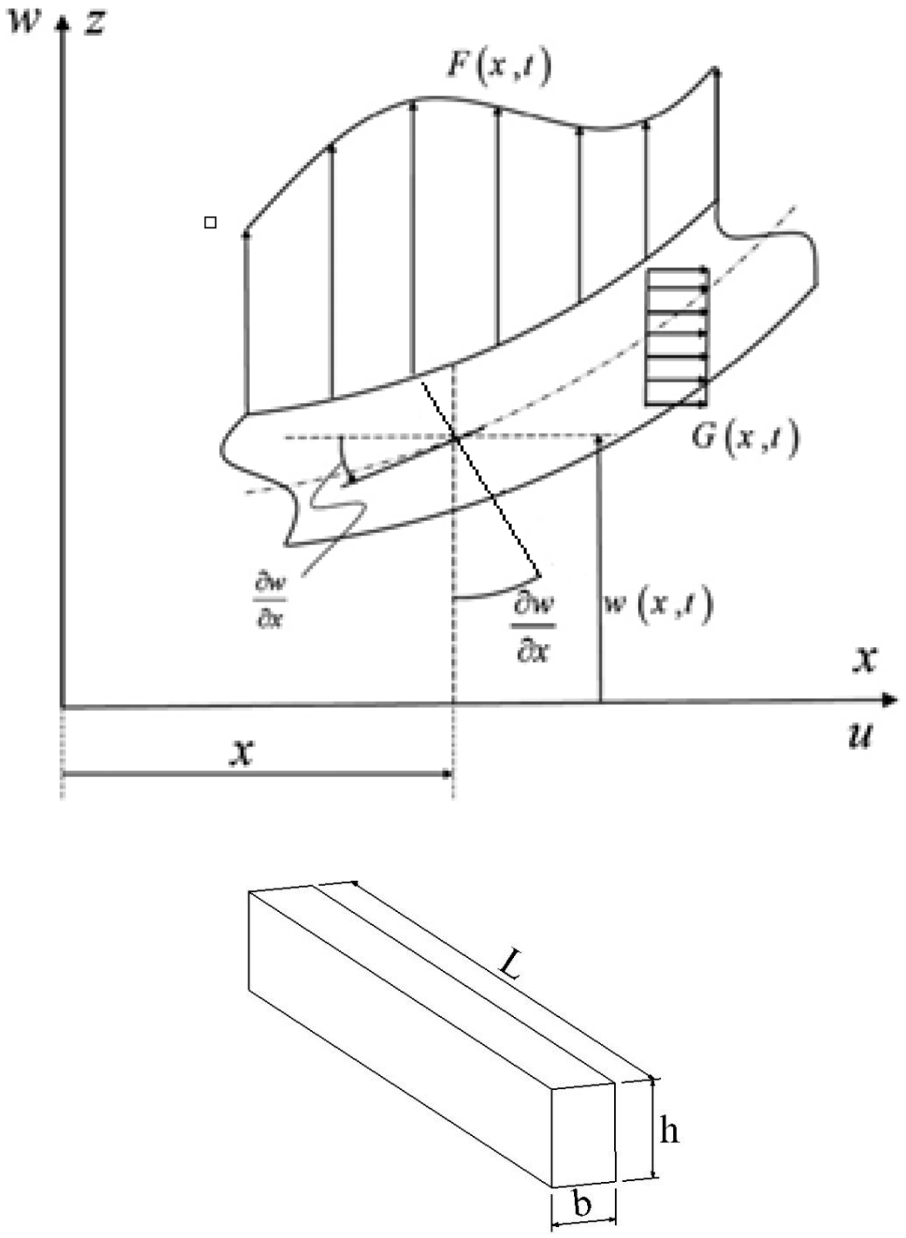

Figure 1. Cartesian coordinate system and loading for Euler-Bernoulli Beam

For a slender beam which has a large aspect ratio (*L/h* & *L/b*) the effect of Poisson's ratio is negligible. This facilitates the formulation of a simple beam theory. By substituting eqn. (2.9) into eqn. (2.2a), it is obtained that

$$\sigma_{xx} = E\left(\frac{\partial u(x,t)}{\partial x} - z\frac{\partial^2 w(x,t)}{\partial x^2}\right), \tag{2.12}$$
$$\sigma_{xy} = \sigma_{yz} = \sigma_{zx} = \sigma_{yy} = \sigma_{zz} = 0,$$

where *E* is Young's modulus.

Then substituting eqn. (2.11) into eqn. (2.4a)

$$m_{xy} = -\mu l^2 \frac{\partial^2 w(x,t)}{\partial x^2}, \tag{2.13}$$
$$m_{yz} = m_{zx} = m_{xx} = m_{yy} = m_{zz} = 0,$$

where μ is shear modulus.

Putting eqn.'s (2.9), (2.11), (2.12), (2.13) into eqn. (2.1) and taking $dv = Adx$

$$U = \frac{1}{2}\int_0^L EA\left(\frac{\partial u(x,t)}{\partial x} - z\frac{\partial^2 w(x,t)}{\partial x^2}\right)^2 + \mu A l^2\left(\frac{\partial^2 w(x,t)}{\partial x^2}\right)^2 dx$$
$$= \frac{1}{2}\int_0^L EA\left(\frac{\partial u(x,t)}{\partial x}\right)^2 + (EI + \mu A l^2)\left(\frac{\partial^2 w(x,t)}{\partial x^2}\right)^2 \text{dx}, \tag{2.14}$$

where *I* is the second moment of inertia $\int_0^L z^2 dA$ and *A* is the cross sectional area of the beam. The coordinate system is chosen such that its origin is located on the centroid of beam. Therefore, the identity $\int_0^L z dA = 0$ is applied to eqn. (2.14).

There is also a work done on the beam by the distributed loads and the edge loads, which is

$$V = \int_0^L [F(x,t)w(x,t) + G(x,t)u(x,t)\,]dx + M_0\frac{\partial w(0,t)}{\partial x} + V_0 w(0,t) + N_0 u(0,t) + M_L\frac{\partial w(L,t)}{\partial x} + V_L w(L,t) + N_L u(L,t), \tag{2.15}$$

where $F(x,t)$ and $G(x,t)$ represent external distributed lateral force per unit length and axial force per unit length respectively. M, V and N represent the bending moment, shear force and axial forces at the boundaries. Subscripts are given to distinguish the boundaries $x = 0$ and $x = L$.

The kinetic energy can be written as

$$T = \frac{1}{2}\int \rho\left[(\frac{\partial u}{\partial t})^2 + (\frac{\partial v}{\partial t})^2 + (\frac{\partial w}{\partial t})^2\right]dV. \tag{2.16}$$

Substituting eqn. (2.7a) into eqn. (2.16) yields

$$T = \frac{1}{2}\int_0^L \left[\rho A(\frac{\partial u(x,t)}{\partial t})^2 + \rho A(\frac{\partial w(x,t)}{\partial t})^2 + \rho I(\frac{\partial w^2(x,t)}{\partial t \partial x})^2\right]dx, \tag{2.17}$$

where ρ is the density of beam. Note that the identity $\int_0^L z dA = 0$ is also applied to eqn. (2.17). Note that rotary inertia is not neglected. Therefore, it appears in the kinetic energy equation.

In order to obtain governing equation of motion, Hamilton's principle is applied

$$\delta \int_{t_1}^{t_2} (T - U + V)dt = 0. \tag{2.18}$$

By substituting eqn.'s (2.14), (2.15), (2.17) into eqn. (2.18)

$$\begin{aligned}\int_{t_1}^{t_2} \Bigg(\frac{1}{2} \Bigg[\int_0^L \left\{ \rho A \left(\frac{\partial u(x,t)}{\partial t} \right)^2 + \rho A \left(\frac{\partial w(x,t)}{\partial t} \right)^2 + \rho I \left(\frac{\partial^2 w(x,t)}{\partial t \partial x} \right)^2 \right\} dx \\ - \int_0^L \left\{ EA \left(\frac{\partial u(x,t)}{\partial x} \right)^2 + (EI + \mu A l^2) \left(\frac{\partial^2 w(x,t)}{\partial x^2} \right)^2 \right\} dx \Bigg] \\ + \int_0^L \{F(x,t)w(x,t) + G(x,t)u(x,t)\} dx + M_0 \frac{\partial w(0,t)}{\partial x} \\ + V_0 w(0,t) + N_0 u(0,t) + M_L \frac{\partial w(L,t)}{\partial x} + V_L w(L,t) \\ + N_L u(L,t) \Bigg) dt = 0.\end{aligned} \tag{2.19}$$

Applying variation operator to the first term of the above equation, and switching the order of variation and partial differentiation

$$\begin{aligned}Term1 \rightarrow \int_{t_1}^{t_2} \int_0^L \Bigg\{ \rho A \left[\frac{\partial u(x,t)}{\partial t} \frac{\partial \delta u(x,t)}{\partial t} + \frac{\partial w(x,t)}{\partial t} \frac{\partial \delta w(x,t)}{\partial t} \right] \\ + \rho I \left(\frac{\partial^2 w(x,t)}{\partial t \partial x} \right) \left(\frac{\partial^2 \delta w(x,t)}{\partial t \partial x} \right) \Bigg\} dx dt.\end{aligned} \tag{2.20}$$

By using some manipulations, Term1 can be reduced to a more tractable form to obtain governing differential equations.

From

$$\frac{\partial}{\partial t}\left\{\delta w\frac{\partial w(x,t)}{\partial t}\right\}=\frac{\partial w(x,t)}{\partial t}\frac{\partial \delta w(x,t)}{\partial t}+\delta w\frac{\partial^2 w(x,t)}{\partial t^2},$$

one obtains

$$\frac{\partial w(x,t)}{\partial t}\frac{\partial \delta w(x,t)}{\partial t}=-\delta w\frac{\partial^2 w(x,t)}{\partial t^2}+\frac{\partial}{\partial t}\left\{\delta w\frac{\partial w(x,t)}{\partial t}\right\}. \tag{2.21}$$

Also from

$$\frac{\partial}{\partial t}\left\{\frac{\partial \delta w(x,t)}{\partial x}\frac{\partial^2 w(x,t)}{\partial t\partial x}\right\}=\frac{\partial^2 \delta w(x,t)}{\partial t\partial x}\frac{\partial^2 w(x,t)}{\partial t\partial x}+\frac{\partial \delta w(x,t)}{\partial x}\frac{\partial^3 w(x,t)}{\partial x\partial t^2},$$

and

$$\frac{\partial}{\partial x}\left\{\delta w\frac{\partial^3 w(x,t)}{\partial x\partial t^2}\right\}=\frac{\partial \delta w(x,t)}{\partial x}\frac{\partial^3 w(x,t)}{\partial x\partial t^2}+\delta w\frac{\partial^4 w(x,t)}{\partial t^2\partial x^2},$$

one obtains

$$\begin{aligned}\frac{\partial^2 \delta w(x,t)}{\partial t\partial x}\frac{\partial^2 w(x,t)}{\partial t\partial x}&=-\frac{\partial}{\partial x}\left\{\delta w\frac{\partial^3 w(x,t)}{\partial x\partial t^2}\right\}\\&+\delta w\frac{\partial^4 w(x,t)}{\partial t^2\partial x^2}+\frac{\partial}{\partial t}\left\{\frac{\partial \delta w(x,t)}{\partial x}\frac{\partial^2 w(x,t)}{\partial t\partial x}\right\}.\end{aligned} \tag{2.22}$$

Now substituting eqn's. (2.21) and (2.22) into eqn. (2.20), and noting that the terms containing *u* can be processed in a similar way to the terms containing *w*, one obtains

$$Term1 \rightarrow \int_{t_1}^{t_2}\int_{0}^{L}\left\{\rho A\left[-\delta u\frac{\partial^2 u(x,t)}{\partial t^2}+\frac{\partial}{\partial t}\left\{\delta u\frac{\partial u(x,t)}{\partial t}\right\}\right]\right.$$
$$+\rho A\left[-\delta w\frac{\partial^2 w(x,t)}{\partial t^2}+\frac{\partial}{\partial t}\left\{\delta w\frac{\partial w(x,t)}{\partial t}\right\}\right]$$
$$+\rho I\left[-\frac{\partial}{\partial x}\left\{\delta w\frac{\partial^3 w(x,t)}{\partial x\partial t^2}\right\}+\delta w\frac{\partial^4 w(x,t)}{\partial t^2\partial x^2}\right.$$
$$\left.\left.+\frac{\partial}{\partial t}\left\{\frac{\partial\delta w(x,t)}{\partial x}\frac{\partial^2 w(x,t)}{\partial t\partial x}\right\}\right]\right\}dxdt.$$

Now one can observe that $\frac{\partial}{\partial t}(\ldots)$ and $\frac{\partial}{\partial x}(\ldots)$ terms can be readily integrated. By doing so and rearranging the terms, Term1 is reduced to the following form

$$Term1 \rightarrow \int_{t1}^{t2}\int_{0}^{L}\left\{\rho A\left[-\delta u\frac{\partial^2 u(x,t)}{\partial t^2}-\delta w\frac{\partial^2 w(x,t)}{\partial t^2}\right]\right.$$
$$\left.+\rho I\left[\delta w\frac{\partial^4 w(x,t)}{\partial t^2\partial x^2}\right]\right\}dx\,dt$$
$$+\int_{0}^{L}\left[\rho A\left[\delta u\frac{\partial u(x,t)}{\partial t}+\delta w\frac{\partial w(x,t)}{\partial t}\right]\right.$$
$$\left.+\rho I\left[\frac{\partial\delta w(x,t)}{\partial x}\frac{\partial^2 w(x,t)}{\partial t\partial x}\right]\right]_{t1}^{t2}dx$$
$$+\int_{t1}^{t2}\left[-\rho I\delta w\frac{\partial^3 w(x,t)}{\partial x\partial t^2}\right]_{0}^{L}dt.$$

Applying variation operator to the second term of equation (2.19)

$$Term2 \rightarrow \int_{t_1}^{t_2}\int_{0}^{L} EA\left(\frac{\partial u(x,t)}{\partial x}\right)\left(\frac{\partial \delta u(x,t)}{\partial x}\right) + (EI + \mu A l^2)\frac{\partial^2 w(x,t)}{\partial x^2}\frac{\partial^2 \delta w(x,t)}{\partial x^2}dxdt. \tag{2.23}$$

Similarly, using the following manipulations,

from

$$\frac{\partial}{\partial x}\left\{\frac{\partial \delta w(x,t)}{\partial x}\frac{\partial^2 w(x,t)}{\partial x^2}\right\} = \frac{\partial^2 \delta w(x,t)}{\partial x^2}\frac{\partial^2 w(x,t)}{\partial x^2} + \frac{\partial \delta w(x,t)}{\partial x}\frac{\partial^3 w(x,t)}{\partial x^3},$$

and

$$\frac{\partial}{\partial x}\left\{\delta w\frac{\partial^3 w(x,t)}{\partial x^3}\right\} = \frac{\partial \delta w(x,t)}{\partial x}\frac{\partial^3 w(x,t)}{\partial x^3} + \delta w\frac{\partial^4 w(x,t)}{\partial x^4}.$$

The last term in eqn. (2.23) is given as

$$\frac{\partial^2 \delta w(x,t)}{\partial x^2}\frac{\partial^2 w(x,t)}{\partial x^2} = \delta w\frac{\partial^4 w(x,t)}{\partial x^4} - \frac{\partial}{\partial x}\left\{\delta w\frac{\partial^3 w(x,t)}{\partial x^3}\right\} + \frac{\partial}{\partial x}\left\{\frac{\partial \delta w(x,t)}{\partial x}\frac{\partial^2 w(x,t)}{\partial x^2}\right\}. \tag{2.24}$$

Also from

$$\frac{\partial}{\partial x}\left\{\delta u\frac{\partial u(x,t)}{\partial x}\right\} = \frac{\partial u(x,t)}{\partial x}\frac{\partial \delta u(x,t)}{\partial x} + \delta u\frac{\partial^2 u(x,t)}{\partial x^2}.$$

The first term in eqn. (2.23) is given as

$$\frac{\partial u(x,t)}{\partial x}\frac{\partial \delta u(x,t)}{\partial x} = -\delta u\frac{\partial^2 u(x,t)}{\partial x^2} + \frac{\partial}{\partial x}\left\{\delta u\frac{\partial u(x,t)}{\partial x}\right\}. \tag{2.25}$$

Substituting eqn.'s (2.24) and (2.25) into eqn. (2.23)

$$\begin{aligned} Term2 \rightarrow \int_{t_1}^{t_2}\int_0^L \left[-EA\delta u\frac{\partial^2 u(x,t)}{\partial x^2} + (EI+\mu Al^2)\delta w\frac{\partial^4 w(x,t)}{\partial x^4}\right] dxdt \\ + \int_{t1}^{t2}\left[EA\delta u\frac{\partial u(x,t)}{\partial x}\right. \\ + (EI+\mu Al^2)\left[-\delta w\frac{\partial^3 w(x,t)}{\partial x^3}\right. \\ \left.\left. + \frac{\partial \delta w(x,t)}{\partial x}\frac{\partial^2 w(x,t)}{\partial x^2}\right]\right]_0^L dt. \end{aligned}$$

In the above equation, the terms which can be readily integrated have been integrated.

Applying variation operator to the third term of eqn. (2.19)

$$\begin{aligned} Term3 \rightarrow \int_{t_1}^{t_2}\left[\int_0^L [F(x,t)\delta w(x,t) + G(x,t)\delta u(x,t)]\,dx + M_0\frac{\partial \delta w(0,t)}{\partial x}\right. \\ + V_0\delta w(0,t) + N_0\delta u(0,t) + M_L\frac{\partial \delta w(L,t)}{\partial x} + V_L\delta w(L,t) \\ \left. + N_L\delta u(L,t)\right] dt \end{aligned} \tag{2.26}$$

Combining $Term1$ & $Term2$ & $Term3$, equation (2.19) becomes

$$
\begin{aligned}
&\int_{t_1}^{t_2}\int_0^L \left[-\rho A\frac{\partial^2 w(x,t)}{\partial t^2}+\rho I\frac{\partial^4 w(x,t)}{\partial t^2\partial x^2}-(EI+\mu Al^2)\frac{\partial^4 w(x,t)}{\partial x^4}\right.\\
&\qquad\left.+F(x,t)\right]\delta w dx dt\\
&+\int_{t_1}^{t_2}\int_0^L\left[-\rho A\frac{\partial^2 u(x,t)}{\partial t^2}+EA\frac{\partial^2 u(x,t)}{\partial x^2}+G(x,t)\right]\delta u dx dt\\
&+\int_0^L\left[\rho A\frac{\partial w(x,t)}{\partial t}\delta w\right]_{t1}^{t2} dx\\
&+\int_0^L\left[\rho A\frac{\partial u(x,t)}{\partial t}\delta u\right]_{t1}^{t2} dx\\
&+\int_0^L\left[\rho I\frac{\partial^2 w(x,t)}{\partial t\partial x}\frac{\partial\delta w(x,t)}{\partial x}\right]_{t1}^{t2} dx\\
&+\int_{t1}^{t2}\left[(EI+\mu Al^2)\frac{\partial^3 w(L,t)}{\partial x^3}-\rho I\frac{\partial^3 w(L,t)}{\partial x\partial t^2}+V_L\right]\delta w(L)dt\\
&+\int_{t1}^{t2}\left[(EI+\mu Al^2)\frac{\partial^3 w(0,t)}{\partial x^3}-\rho I\frac{\partial^3 w(0,t)}{\partial x\partial t^2}+V_0\right]\delta w(0)dt\\
&+\int_{t1}^{t2}\left[-EA\frac{\partial u(L,t)}{\partial x}+N_L\right]\delta u(L)dt\\
&+\int_{t1}^{t2}\left[-EA\frac{\partial u(0,t)}{\partial x}+N_0\right]\delta u(0)dt\\
&+\int_{t1}^{t2}\left[-(EI+\mu Al^2)\frac{\partial^2 w(L,t)}{\partial x^2}+M_L\right]\frac{\partial\delta w(L)}{\partial x}dt\\
&+\int_{t1}^{t2}\left[-(EI+\mu Al^2)\frac{\partial^2 w(0,t)}{\partial x^2}+M_0\right]\frac{\partial\delta w(0)}{\partial x}dt=0\,.
\end{aligned}
\tag{2.27}
$$

The first two terms of eqn. (2.27) contain arbitrary variations of δu and δw which are not necessarily zero. In order to satisfy eqn. (2.27), it is therefore required that their

coefficients enclosed in square brackets should be equal to zero. These conditions give the governing equations (equations of motion) for the beam.

$$\delta w: \quad (EI + \mu A l^2)\frac{\partial^4 w(x,t)}{\partial x^4} + \rho A \frac{\partial^2 w(x,t)}{\partial t^2} - \rho I \frac{\partial^4 w(x,t)}{\partial t^2 \partial x^2} = F(x,t), \tag{2.28}$$

$$\delta u: \quad -EA\frac{\partial^2 u(x,t)}{\partial x^2} + \rho A \frac{\partial^2 u(x,t)}{\partial t^2} = G(x,t). \tag{2.29}$$

Note that, if rotary inertia is neglected, the term $\rho I \frac{\partial^4 w(x,t)}{\partial t^2 \partial x^2}$ in equation (2.28) vanishes. Moreover, obtained equations of motions are in agreement with the ones in the literature such as [73], [77] and [82].

Hamilton's principle is based on the premise [112] that the actual and the varied paths intersect at the instants t_1 and t_2 so that at these instants $\delta u(t_1) = \delta u(t_2) = 0$ and $\delta w(t_1) = \delta w(t_2) = 0$. For this reason, the time integrated third, fourth and the fifth terms in eqn. (2.27) become zero.

On the other hand, the last three terms give the boundary conditions for the beam at *x=0* and *x=L*. These boundary conditions, prescribed at $x = L$ and $x = 0$ are

$$EA\frac{\partial u(0,t)}{\partial x} = N_0 = Q_1, \tag{2.30a}$$

$$(EI + \mu A l^2)\frac{\partial^3 w(0,t)}{\partial x^3} - \rho I \frac{\partial^3 w(0,t)}{\partial x \partial t^2} = -V_0 = Q_2, \tag{2.30b}$$

$$(EI + \mu Al^2)\frac{\partial^2 w(0,t)}{\partial x^2} = M_0 = Q_3, \tag{2.30c}$$

$$EA\frac{\partial u(L,t)}{\partial x} = N_L = Q_4, \tag{2.30d}$$

$$(EI + \mu Al^2)\frac{\partial^3 w(L,t)}{\partial x^3} - \rho I\frac{\partial^3 w(L,t)}{\partial x \partial t^2} = -V_L = Q_5, \tag{2.30e}$$

$$(EI + \mu Al^2)\frac{\partial^2 w(L,t)}{\partial x^2} = M_L = Q_6, \tag{2.30f}$$

where Q_1 and Q_4 denote the axial forces, Q_2 and Q_5 denote the shear forces, Q_3 and Q_6 denote the bending moment. Note that in eqn. (2.28), it can be seen that EI, ρI and ρA are related with the classical beam model. However, μAl^2 is related with the MCST beam model, which represents the size effect. If material length scale parameter is set to zero ($l = 0$), the equation becomes classical governing equation of motion of an Euler-Bernoulli beam. Similarly, if material length scale parameter is set to zero ($l = 0$), boundary conditions eqn. (2.30a) are also reduces to that of classical Euler-Bernoulli beam.

CHAPTER 3

NUMERICAL SOLUTION

3.1 Introduction

In this thesis, Finite Element Method (FEM) is used to obtain numerical solution. The basic steps of FEM as applied to this thesis can be outlined as follows. The first step is idealization by elements where the solution domain is divided into elements. In the second step discretization by nodes and interpolation functions is done. In step three, elemental stiffness and mass matrices are obtained either directly from a variational statement (by using Ritz method) or from a constructed weak form of the governing differential equations (by using Galerkin method). These formulations are given in this chapter. In step four, elemental stiffness and mass matrices are assembled to form overall system matrices. In step five, boundary conditions are introduced and in the sixth step, the solution (i.e. displacements for static loading, eigenvalues for free vibration problems) is obtained. In step seven, forces (stresses) for static problems and eigen vectors for free vibration problems are obtained. The fourth, fifth, sixth and seventh steps for the problem under consideration are implemented in the developed code.

Before starting the numerical solution, it is necessary to emphasize the difference between Ritz method and Galerkin method. Although, the Ritz method can be directly applied to the variational form of energy equation [19] to obtain mass and stiffness matrices, Galerkin method is utilized in this study. There are mainly two reasons of choosing Galerkin approach.

The first reason is that when the weak form of energy equation is directly used with Ritz method, there is no need to obtain equation of motion, in general. However, the papers

in the literature that prefer to use analytical solution instead of finite element solution obtain the equation of motion. In order to compare the formulation in this work with those papers, deriving the equation of motion is necessary.

The second reason is that, in Reddy [113], it is stated that the two methods, Ritz and Galerkin, give the same results when the two conditions stated below are satisfied:

1. All boundary conditions are essential type boundary conditions so that the weighted integral form of Galerkin method reduces to weak form of Ritz method.
2. Approximation function of Galerkin method is used for Ritz method.

From those two listed remarks in Reddy [113], it is concluded that, in our case, Galerkin method gives the same solution with Ritz method if the same approximation functions are used. Moreover, Galerkin method is easily applied to all type of problems and boundary conditions.

Therefore, Galerkin Method is used throughout formulations in this study.

In this chapter, the numerical solution part is divided into 2 sections: Static behavior and dynamic behavior.

3.2 Static Behavior

After omitting time dependent terms, the static parts of equations (2.28) and (2.29) can be expressed as

$$\delta w: \quad (EI + \mu A l^2)\frac{\partial^4 w(x)}{\partial x^4} - F(x) = 0, \tag{3.1}$$

$$\delta u: \quad EA\frac{\partial^2 u(x,t)}{\partial x^2} + G(x,t) = 0. \tag{3.2}$$

In order to move on with finite element approach and employ Galerkin method, weight functions are applied to both eqn. (3.1) and eqn. (3.2)

$$\int_0^L \left[(EI + \mu Al^2)\frac{\partial^4 w(x)}{\partial x^4} - F(x)\right] X_1 dx = 0, \tag{3.3}$$

$$\int_0^L \left[EA\frac{\partial^2 u(x)}{\partial x^2} + G(x)\right] X_2 dx = 0, \tag{3.4}$$

where X_1 and X_2 denotes the weight functions.

After distributing weight function, equation (3.3) becomes

$$\int_0^L \left[(EI + \mu Al^2)\frac{\partial^4 w(x)}{\partial x^4} X_1 - F(x)X_1\right] dx = 0. \tag{3.5}$$

Using the following manipulations

$$\frac{\partial}{\partial x}\left\{X_1(EI + \mu Al^2)\frac{\partial^3 w(x)}{\partial x^3}\right\} = \frac{\partial X_1}{\partial x}(EI + \mu Al^2)\frac{\partial^3 w(x)}{\partial x^3} + X_1(EI + \mu Al^2)\frac{\partial^4 w(x)}{\partial x^4},$$

and

$$\frac{\partial}{\partial x}\left\{\frac{\partial X_1}{\partial x}(EI + \mu Al^2)\frac{\partial^2 w(x)}{\partial x^2}\right\} = \frac{\partial^2 X_1}{\partial x^2}(EI + \mu Al^2)\frac{\partial^2 w(x)}{\partial x^2} + \frac{\partial X_1}{\partial x}(EI + \mu Al^2)\frac{\partial^3 w(x)}{\partial x^3},$$

one obtains,

$$X_1(EI+\mu Al^2)\frac{\partial^4 w(x)}{\partial x^4}=\frac{\partial}{\partial x}\left\{X_1(EI+\mu Al^2)\frac{\partial^3 w(x)}{\partial x^3}\right\} - \frac{\partial}{\partial x}\left\{\frac{\partial X_1}{\partial x}(EI+\mu Al^2)\frac{\partial^2 w(x)}{\partial x^2}\right\}+\frac{\partial^2 X_1}{\partial x^2}(EI+\mu Al^2)\frac{\partial^2 w(x)}{\partial x^2}. \tag{3.6}$$

Substituting eqn. (3.6) into eqn. (3.5)

$$\int_0^L\left[\frac{\partial}{\partial x}\left\{X_1(EI+\mu Al^2)\frac{\partial^3 w(x)}{\partial x^3}\right\}-\frac{\partial}{\partial x}\left\{\frac{\partial X_1}{\partial x}(EI+\mu Al^2)\frac{\partial^2 w(x)}{\partial x^2}\right\} +\frac{\partial^2 X_1}{\partial x^2}(EI+\mu Al^2)\frac{\partial^2 w(x)}{\partial x^2}-F(x)X_1\right]dx=0.$$

Integrating the terms which are differentiated with respect to *x*

$$\int_0^L\left[\frac{\partial^2 X_1}{\partial x^2}(EI+\mu Al^2)\frac{\partial^2 w(x)}{\partial x^2}-F(x)X_1\right]dx + \left[X_1(EI+\mu Al^2)\frac{\partial^3 w(x)}{\partial x^3}-\frac{\partial X_1}{\partial x}(EI+\mu Al^2)\frac{\partial^2 w(x)}{\partial x^2}\right]_0^L = 0. \tag{3.7}$$

Similarly, after distributing weight function, eqn. (3.4) becomes

$$\int_0^L\left[EA\frac{\partial^2 u(x)}{\partial x^2}X_2+G(x)X_2\right]dx=0. \tag{3.8}$$

Using the following manipulation

$$\frac{\partial}{\partial x}\left\{X_2\frac{\partial u(x)}{\partial x}\right\} = \frac{\partial X_2}{\partial x}\frac{\partial u(x)}{\partial x} + X_2\frac{\partial^2 u(x)}{\partial x^2},$$

$$X_2\frac{\partial^2 u(x)}{\partial x^2} = \frac{\partial}{\partial x}\left\{X_2\frac{\partial u(x)}{\partial x}\right\} - \frac{\partial X_2}{\partial x}\frac{\partial u(x)}{\partial x}. \tag{3.9}$$

Substituting eqn. (3.9) into eqn. (3.8)

$$\int_0^L EA\left[\frac{\partial}{\partial x}\left\{X_2\frac{\partial u(x)}{\partial x}\right\} - \frac{\partial X_2}{\partial x}\frac{\partial u(x)}{\partial x}\right]dx = 0,$$

and integrating the differentiated term

$$\int_0^L \left[EA\frac{\partial X_2}{\partial x}\frac{\partial u(x)}{\partial x} - G(x)X_2\right]dx - EA\left[X_2\frac{\partial u(x)}{\partial x}\right]_0^L = 0. \tag{3.10}$$

In order to obtain the finite element model, the length of the beam is discretized into set of smaller elements and the weak form is applied on one of those elements. Element nodes and degrees of freedom of the nodes are given in Figure 2.

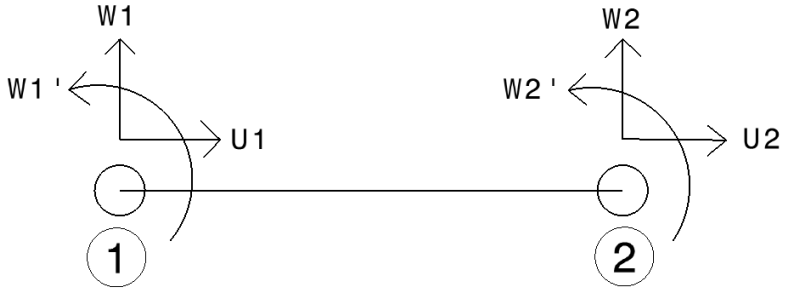

Figure 2. 3-DOF Finite element model

When the highest order derivative of the unknown function in a variational statement is *m*, this is referred to a C^{m-1} problem. For example in eqn. (2.27), we have $\frac{\partial^4 w}{\partial x^4}$ therefore *m*=4 and we have a C^3 problem. This means that *w*, $\frac{\partial w}{\partial x}$, $\frac{\partial^2 w}{\partial x^2}$,and $\frac{\partial^3 w}{\partial x^3}$ must be continuous. Similarly, for *u* we have a C^1 problem (*u*, $\frac{\partial u}{\partial x}$ must be continuous). These should be taken into account in FEM discretization of the problem.

Then interpolation of *w* can be done by following equation

$$w(x) = \sum_{j}^{4} w_j^e \, \emptyset_j^e, \tag{3.11}$$

where w_j^e denotes the nodal degrees of freedom. $\emptyset_j^e$ denotes the Hermite Cubic Interpolation Functions [113]

$$\emptyset_1^e = 1 - 3\left(\frac{x - x_e}{h_e}\right)^2 + 2\left(\frac{x - x_e}{h_e}\right)^3,$$

$$\emptyset_2^e = -(x - x_e)\left(1 - \frac{x - x_e}{h_e}\right)^2,$$

$$\emptyset_3^e = 3\left(\frac{x - x_e}{h_e}\right)^2 - 2\left(\frac{x - x_e}{h_e}\right)^3,$$

$$\emptyset_4^e = -(x - x_e)\left[\left(\frac{x - x_e}{h_e}\right)^2 - \frac{x - x_e}{h_e}\right],$$

where h_e is the length of an element with $x_{e+1} = x_e + h_e$ as shown in Figure 3.

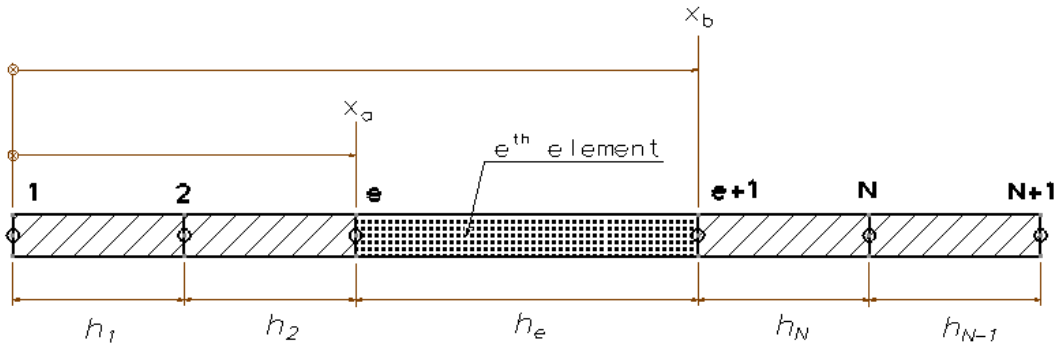

Figure 3. Finite element discretization of the beam

For axial deflection and vibration below linear interpolation functions are used

$$u(x) = \sum_{j}^{2} u_i^e \, \emptyset_{iL}^e, \tag{3.12}$$

$$\emptyset_{1L}^e = 1 - \frac{x - x_e}{h_e},$$

$$\emptyset_{2L}^e = \frac{x - x_e}{h_e}.$$

Substituting equations eqn. (3.11) and eqn. (3.12) into eqn. (3.7) and eqn. (3.10), and recognizing that according to Galerkin method X_1 and X_2 are respectively taken as $\emptyset_{\mathrm{j}}^{\mathrm{e}}$ and $\emptyset_{\mathrm{jL}}^{\mathrm{e}}$, the following is obtained

$$\sum_{i}^{4} w_i^e \left\{ \int_{x_a}^{x_b} \left[(EI + \mu A l^2) \frac{\partial^2 \emptyset_i^e}{\partial x^2} \frac{\partial^2 \emptyset_j^e}{\partial x^2} - F(x) \emptyset_{\mathrm{j}}^{\mathrm{e}} \right] dx \right.$$

$$\left. + \left(\emptyset_j^e \left((EI + \mu A l^2) \frac{\partial^3 \emptyset_i^e}{\partial x^3} \right) \right) \Bigg|_0^L - \left(\frac{\partial \emptyset_j^e}{\partial x} (EI + \mu A l^2) \frac{\partial^2 \emptyset_i^e}{\partial x^2} \right) \Bigg|_0^L \right\} = 0, \tag{3.13}$$

for $j = 1,2,3,4$

$$\sum_{i}^{2} u_i^e \left\{ \int_{x_a}^{x_b} \left[EA \frac{\partial \emptyset_{jL}^e}{\partial x} \frac{\partial \emptyset_{iL}^e}{\partial x} - G(x) \emptyset_{jL}^e \right] dx - EA \emptyset_{jL}^e \frac{\partial \emptyset_{iL}^e}{\partial x} \Big|_0^L \right\} = 0, \qquad (3.14)$$

$$\text{for } \; j = 1,2$$

The equations (3.13) and (3.14) can be represented in general form

$$[\boldsymbol{K}^e]\{u^e\} - \{\boldsymbol{F}^e\} = 0,$$

where for transverse motion, *w*

$$\boldsymbol{K}_{ij}^e = \int_0^L \left[(EI + \mu A l^2) \frac{\partial^2 \emptyset_i^e}{\partial x^2} \frac{\partial^2 \emptyset_j^e}{\partial x^2} \right] dx,$$

$$\boldsymbol{F}_i^e = \int_0^L \left[F(x) \emptyset_{\mathrm{j}}^{\mathrm{e}} \right] dx + \; \boldsymbol{Q}_i^e.$$

For axial motion, *u*

$$\boldsymbol{K}_{\boldsymbol{L}ij}^e = \int_0^L \left[EA \frac{\partial \emptyset_{iL}^e}{\partial x} \frac{\partial \emptyset_{jL}^e}{\partial x} \right] dx,$$

$$\boldsymbol{F}_{Li}^e = \int_0^L \left[G(x) \emptyset_{\mathrm{jL}}^{\mathrm{e}} \right] dx + \; \boldsymbol{Q}_i^e.$$

Basically, $\boldsymbol{K}$, $\boldsymbol{K_L}$ are the elemental stiffness matrices, $\boldsymbol{F}$, $\boldsymbol{F_L}$ are the force vectors and $\boldsymbol{Q}$'s are the generalized forces. Note that time dependent terms in generalized force equation are omitted since this part covers only the static solution.

By using MATLAB R2015a, the combined stiffness matrix for transverse and axial motion is obtained as

$$\boldsymbol{K}=\begin{bmatrix} \frac{EA}{L} & 0 & 0 & -\frac{EA}{L} & 0 & 0 \\ 0 & 12\frac{(EI)}{L^3}(1+a) & 6\frac{(EI)}{L^2}(1+a) & 0 & -12\frac{(EI)}{L^3}(1+a) & 6\frac{(EI)}{L^2}(1+a) \\ 0 & 6\frac{(EI)}{L^2}(1+a) & 4\frac{(EI)}{L}(1+a) & 0 & -6\frac{(EI)}{L^2}(1+a) & 2\frac{(EI)}{L}(1+a) \\ -\frac{EA}{L} & 0 & 0 & \frac{EA}{L} & 0 & 0 \\ 0 & -12\frac{(EI)}{L^3}(1+a) & -6\frac{(EI)}{L^2}(1+a) & 0 & 12\frac{(EI)}{L^3}(1+a) & -6\frac{(EI)}{L^2}(1+a) \\ 0 & 6\frac{(EI)}{L^2}(1+a) & 2\frac{(EI)}{L}(1+a) & 0 & -6\frac{(EI)}{L^2}(1+a) & 4\frac{(EI)}{L}(1+a) \end{bmatrix},$$

where $a=\frac{\mu A l^2}{EI}$. Also, corresponded force vector is obtained as follows

$$\boldsymbol{F}=[\frac{GL}{2} \quad \frac{FL}{2} \quad \frac{FL^2}{12} \quad \frac{GL}{2} \quad \frac{FL}{2} \quad -\frac{FL^2}{12}]^T.$$

Note that, as seen from above matrices, the bending and axial stiffness of beam are uncoupled.

Also note that, distributed load is considered as uniform throughout the beam.

Moreover, the corresponding displacement vector can be expressed as,

$$u=[u_1 \quad w_1 \quad w'_1 \quad u_2 \quad w_2 \quad w'_2]^T$$

where u is the axial, w is the transverse and w' is the angular displacements as shown in Figure 2. Subscripts describe the two nodes of an element.

The developed Euler Bernoulli beam model based on MCST reduces to the classical Euler Bernoulli beam model. By letting $l=0$, the stiffness matrix reduces to

$$\boldsymbol{K} = \begin{bmatrix} \frac{EA}{L} & 0 & 0 & -\frac{EA}{L} & 0 & 0 \\ 0 & 12\frac{(EI)}{L^3} & 6\frac{(EI)}{L^2} & 0 & -12\frac{(EI)}{L^3} & 6\frac{(EI)}{L^2} \\ 0 & 6\frac{(EI)}{L^2} & 4\frac{(EI)}{L} & 0 & -6\frac{(EI)}{L^2} & 2\frac{(EI)}{L} \\ -\frac{EA}{L} & 0 & 0 & \frac{EA}{L} & 0 & 0 \\ 0 & -12\frac{(EI)}{L^3} & -6\frac{(EI)}{L^2} & 0 & 12\frac{(EI)}{L^3} & -6\frac{(EI)}{L^2} \\ 0 & 6\frac{(EI)}{L^2} & 2\frac{(EI)}{L} & 0 & -6\frac{(EI)}{L^2} & 4\frac{(EI)}{L} \end{bmatrix},$$

which is the stiffness matrix for a classical Euler-Bernoulli beam model.

3.3 Dynamic Behavior

Without any external excitation, the equations (2.28) and (2.29) can be expressed as

$$(EI + \mu Al^2)\frac{\partial^4 w(x,t)}{\partial x^4} + \rho A\frac{\partial^2 w(x,t)}{\partial t^2} - \rho I\frac{\partial^4 w(x,t)}{\partial t^2 \partial x^2} = 0, \tag{3.15}$$

$$-EA\frac{\partial^2 u(x,t)}{\partial x^2} + \rho A\frac{\partial^2 u(x,t)}{\partial t^2} = 0. \tag{3.16}$$

By assuming periodic motion, displacements can be expressed as

$$w(x,t) = w_0(x)e^{i\omega t} \qquad \text{and} \qquad u(x,t) = u_0(x)e^{i\omega t}, \tag{3.17}$$

where ω is the excitation frequency of vibratory motion and $w_0(x)$ and $u_0(x)$ are the amplitudes in z and x directions which depend on x-coordinate. Inserting eqn. (3.17) into eqn. (3.15) and eqn. (3.16) leads to

$$(EI + \mu Al^2)e^{i\omega t}\frac{\partial^4 w_0(x)}{\partial x^4} - m\omega^2 w_0(x)e^{i\omega t} + \rho I\omega^2\frac{\partial^2 w_0(x)}{\partial x^2}e^{i\omega t} = 0,$$

$$e^{i\omega t}\left\{(EI + \mu Al^2)\frac{\partial^4 w_0(x)}{\partial x^4} - m\omega^2 w_0(x) + \rho I\omega^2\frac{\partial^2 w_0(x)}{\partial x^2}\right\} = 0.$$

Setting the term enclosed in the brackets equal to zero

$$(EI + \mu Al^2)\frac{\partial^4 w_0(x)}{\partial x^4} - m\omega^2 w_0(x) + \rho I\omega^2\frac{\partial^2 w_0(x)}{\partial x^2} = 0, \tag{3.18}$$

$$-EAe^{i\omega t}\frac{\partial^2 u_0(x)}{\partial x^2} - m\omega^2 u_0(x)e^{i\omega t} = 0.$$

Similarly

$$e^{i\omega t}\left[EA\frac{\partial^2 u_0(x)}{\partial x^2} + m\omega^2 u_0(x)\right] = 0,$$

$$EA\frac{\partial^2 u_0(x)}{\partial x^2} + m\omega^2 u_0(x) = 0, \tag{3.19}$$

where $m = \rho A$ mass per unit length.

Equations.(3.18) and (3.19) are the uncoupled strong forms of the governing equations for the displacement distribution of a vibrating beam.

Similar to static part of the derivation, in order to move on with finite element approach and employ Galerkin method, weight functions are applied to both eqn. (3.18) and eqn. (3.19)

$$\int_0^L \left[-m\lambda w_0(x) + \rho I\lambda \frac{\partial^2 w_0(x)}{\partial x^2} + (EI + \mu A l^2)\frac{\partial^4 w_0(x)}{\partial x^4}\right] X_1 dx = 0, \tag{3.20}$$

$$\int_0^L \left[m\lambda u_0(x) + EA\frac{\partial^2 u_0(x)}{\partial x^2}\right] X_2 dx = 0, \tag{3.21}$$

where X_1 and X_2 denotes the weight functions and $\lambda = \omega^2$.

First term of equation eqn. (3.20) becomes

$$Term1 \rightarrow \int_0^L -m\lambda w_0(x) X_1 dx.$$

Second term of eqn. (3.20) can be written as

$$Term2 \rightarrow \int_0^L \rho I\lambda \frac{\partial^2 w_0(x)}{\partial x^2} X_1 dx$$

Using the following manipulation

$$\frac{\partial}{\partial x}\left\{X_1 \frac{\partial w_0(x)}{\partial x}\right\} = \frac{\partial X_1}{\partial x}\frac{\partial w_0(x)}{\partial x} + X_1 \frac{\partial^2 w_0(x)}{\partial x^2},$$

$$X_1 \frac{\partial^2 w_0(x)}{\partial x^2} = \frac{\partial}{\partial x}\left\{X_1 \frac{\partial w_0(x)}{\partial x}\right\} - \frac{\partial X_1}{\partial x}\frac{\partial w_0(x)}{\partial x}. \tag{3.22}$$

Substituting eqn. (3.22) into $Term2$

$$Term2 \rightarrow \int_0^L \rho I\lambda \frac{\partial}{\partial x}\left\{X_1 \frac{\partial w_0(x)}{\partial x}\right\} - \rho I\lambda \frac{\partial X_1}{\partial x}\frac{\partial w_0(x)}{\partial x}dx$$

$$Term2 \rightarrow \int_0^L -\rho I\lambda \frac{\partial X_1}{\partial x}\frac{\partial w_0(x)}{\partial x}dx + \rho I\lambda \left[X_1 \frac{\partial w_0(x)}{\partial x}\right]_0^L$$

Third term of eqn. (3.20) becomes

$$Term3 \rightarrow \int_0^L (EI + \mu Al^2)\frac{\partial^4 w_0(x)}{\partial x^4} X_1 dx \tag{3.23}$$

Using the following manipulations

$$\frac{\partial}{\partial x}\left\{X_1(EI + \mu Al^2)\frac{\partial^3 w_0(x)}{\partial x^3}\right\} = \frac{\partial X_1}{\partial x}(EI + \mu Al^2)\frac{\partial^3 w_0(x)}{\partial x^3} + X_1(EI + \mu Al^2)\frac{\partial^4 w_0(x)}{\partial x^4},$$

$$\frac{\partial}{\partial x}\left\{\frac{\partial X_1}{\partial x}(EI + \mu Al^2)\frac{\partial^2 w_0(x)}{\partial x^2}\right\} = \frac{\partial^2 X_1}{\partial x^2}(EI + \mu Al^2)\frac{\partial^2 w_0(x)}{\partial x^2} + \frac{\partial X_1}{\partial x}(EI + \mu Al^2)\frac{\partial^3 w_0(x)}{\partial x^3}.$$

One can write

$$X_1(EI+\mu Al^2)\frac{\partial^4 w_0(x)}{\partial x^4}=\frac{\partial}{\partial x}\left\{X_1(EI+\mu Al^2)\frac{\partial^3 w_0(x)}{\partial x^3}\right\}$$
$$-\frac{\partial}{\partial x}\left\{\frac{\partial X_1}{\partial x}(EI+\mu Al^2)\frac{\partial^2 w_0(x)}{\partial x^2}\right\}+\frac{\partial^2 X_1}{\partial x^2}(EI+\mu Al^2)\frac{\partial^2 w_0(x)}{\partial x^2}. \quad (3.24)$$

Substituting eqn. (3.24) into eqn. (3.23)

$$Term3 \rightarrow \int_0^L \frac{\partial}{\partial x}\left\{X_1(EI+\mu Al^2)\frac{\partial^3 w_0(x)}{\partial x^3}\right\}$$
$$-\frac{\partial}{\partial x}\left\{\frac{\partial X_1}{\partial x}(EI+\mu Al^2)\frac{\partial^2 w_0(x)}{\partial x^2}\right\}$$
$$+\frac{\partial^2 X_1}{\partial x^2}(EI+\mu Al^2)\frac{\partial^2 w_0(x)}{\partial x^2}dx,$$
$$Term3 \rightarrow \int_0^L \frac{\partial^2 X_1}{\partial x^2}(EI+\mu Al^2)\frac{\partial^2 w_0(x)}{\partial x^2}dx+X_1(EI+\mu Al^2)\frac{\partial^3 w_0(x)}{\partial x^3}$$
$$-\frac{\partial X_1}{\partial x}(EI+\mu Al^2)\frac{\partial^2 w_0(x)}{\partial x^2}.$$

Combining $Term1$ & $Term2$ & $Term3$, equation (3.20) becomes

$$\int_0^L\left[(EI+\mu Al^2)\frac{\partial^2 w_0(x)}{\partial x^2}\frac{\partial^2 X_1}{\partial x^2}-m\lambda X_1 w_0(x)-\rho I\lambda\frac{\partial X_1}{\partial x}\frac{\partial w_0(x)}{\partial x}\right]dx$$
$$+\left[X_1\left(\rho I\lambda\frac{\partial w_0(x)}{\partial x}+(EI+\mu Al^2)\frac{\partial^3 w_0(x)}{\partial x^3}\right)\right]_0^L \quad (3.25)$$
$$-\left[\frac{\partial X_1}{\partial x}(EI+\mu Al^2)\frac{\partial^2 w_0(x)}{\partial x^2}\right]_0^L=0.$$

Similarly, first term of equation eqn. (3.21)

$$Term1 \rightarrow \int_0^L m\lambda u_0(x) X_2 dx.$$

Then the second term of eqn. (3.21)

$$Term2 \rightarrow \int_0^L EA \frac{\partial^2 u_0(x)}{\partial x^2} X_2 dx. \tag{3.26}$$

Using the following manipulation

$$\frac{\partial}{\partial x}\left\{X_2 \frac{\partial u_0(x)}{\partial x}\right\} = \frac{\partial X_2}{\partial x}\frac{\partial u_0(x)}{\partial x} + X_2 \frac{\partial^2 u_0(x)}{\partial x^2},$$

$$X_2 \frac{\partial^2 u_0(x)}{\partial x^2} = \frac{\partial}{\partial x}\left\{X_2 \frac{\partial u_0(x)}{\partial x}\right\} - \frac{\partial X_2}{\partial x}\frac{\partial u_0(x)}{\partial x}. \tag{3.27}$$

Substituting eqn. (3.27) into eqn. (3.26)

$$Term2 \rightarrow \int_0^L EA \left[\frac{\partial}{\partial x}\left\{X_2 \frac{\partial u_0(x)}{\partial x}\right\} - \frac{\partial X_2}{\partial x}\frac{\partial u_0(x)}{\partial x}\right] dx,$$

$$Term2 \rightarrow \int_0^L -EA \frac{\partial X_2}{\partial x}\frac{\partial u_0(x)}{\partial x} dx + EA\left[X_2 \frac{\partial u_0(x)}{\partial x}\right]_0^L.$$

Combining $Term1$ & $Term2$ eqn. (3.21) can be expressed as

$$\int_0^L \left[EA \frac{\partial X_2}{\partial x}\frac{\partial u_0(x)}{\partial x} - m\lambda X_2 u_0(x)\right] dx - EAX_2 \frac{\partial u_0(x)}{\partial x}\Big|_0^L = 0. \tag{3.28}$$

Similar to static part of the derivation, discretization is applied with finite element model shown in figure 2 and figure 3 in previous section. The interpolation can be done by following equations for transverse and axial vibrations, respectively

$$w_0(x) = \sum_{j}^{4} w_j^e \, \emptyset_j^e, \tag{3.29}$$

$$u_o(x) = \sum_{j}^{2} u_i^e \, \emptyset_{iL}^e. \tag{3.30}$$

Note that, the same Hermite interpolation functions are used in the above expressions. Substituting equations (3.29) and (3.30) into equations (3.25) and (3.28), and recognizing that according to Galerkin method X_1 and X_2 are respectively taken as $\emptyset_{\mathrm{j}}^{\mathrm{e}}$ and $\emptyset_{\mathrm{jL}}^{\mathrm{e}}$, the following is obtained

$$\sum_{i}^{4} w_i^e \left\{ \int_{x_a}^{x_b} \left[(EI + \mu A l^2) \frac{\partial^2 \emptyset_i^e}{\partial x^2} \frac{\partial^2 \emptyset_j^e}{\partial x^2} - m\lambda \emptyset_j^e \emptyset_i^e - \rho I \lambda \frac{\partial \emptyset_j^e}{\partial x} \frac{\partial \emptyset_i^e}{\partial x} \right] dx \right.$$
$$\left. + \left(\emptyset_j^e \left(\rho I \lambda \frac{\partial \emptyset_i^e}{\partial x} + (EI + \mu A l^2) \frac{\partial^3 \emptyset_i^e}{\partial x^3} \right) \right) \Bigg|_0^L - \left(\frac{\partial \emptyset_j^e}{\partial x} (EI + \mu A l^2) \frac{\partial^2 \emptyset_i^e}{\partial x^2} \right) \Bigg|_0^L \right\} \tag{3.31}$$
$$= 0,$$
$$\text{for} \quad j = 1,2,3,4$$

$$\sum_{i}^{2} u_i^e \left\{ \int_{x_a}^{x_b} \left[EA \frac{\partial \emptyset_{jL}^e}{\partial x} \frac{\partial \emptyset_{iL}^e}{\partial x} - m\lambda \emptyset_{jL}^e \emptyset_{iL}^e \right] dx - EA \emptyset_{jL}^e \frac{\partial \emptyset_{iL}^e}{\partial x} \Bigg|_0^L \right\} = 0, \tag{3.32}$$
$$\text{for} \quad j = 1,2$$

Above equations can be represented in the general form for free vibration

$$[\boldsymbol{K}^e - \lambda \boldsymbol{M}^e]\{u^e\} = 0,$$

where for transverse motion, *w*

$$\boldsymbol{K}_{ij}^e = \int_0^L \left[(EI + \mu A l^2) \frac{\partial^2 \emptyset_i^e}{\partial x^2} \frac{\partial^2 \emptyset_j^e}{\partial x^2} \right] dx$$

$$\boldsymbol{M_t}_{ij}^e = \int_0^L \left[m \emptyset_i^e \emptyset_j^e \right] dx$$

$$\boldsymbol{M_\theta}_{ij}^e = \int_0^L \left[\rho I \frac{\partial \emptyset_i^e}{\partial x} \frac{\partial \emptyset_j^e}{\partial x} \right] dx$$

$$\boldsymbol{M} = \boldsymbol{M_t} + \boldsymbol{M_\theta}$$

For axial motion, *u*;

$$\boldsymbol{K}_{\boldsymbol{L}ij}^e = \int_0^L \left[EA \frac{\partial \emptyset_{iL}^e}{\partial x} \frac{\partial \emptyset_{jL}^e}{\partial x} \right] dx$$

$$\boldsymbol{M_t}_{\boldsymbol{L}ij}^e = \int_0^L \left[m \emptyset_{iL}^e \emptyset_{jL}^e \right] dx$$

$$\boldsymbol{M_\theta}_{\boldsymbol{L}ij}^e = 0$$

$$\boldsymbol{M_L} = \boldsymbol{M_{t_L}} + \boldsymbol{M_{\theta_L}}$$

Basically, $\boldsymbol{K}$, $\boldsymbol{K_L}$ are the elemental stiffness matrices, which are already obtained in the static part of this work, $\boldsymbol{M_t}, \boldsymbol{M_{t_L}}$ are the mass matrices resulting from the translational inertia and $\boldsymbol{M_\theta}, \boldsymbol{M_{\theta_L}}$ are the mass matrices resulting from the rotational inertia, $\boldsymbol{M}$, $\boldsymbol{M_L}$ are the total mass matrices.

By using MATLAB R2015a, the combined mass matrices for transverse and axial motion are obtained as follows

$$\boldsymbol{M_t} = \frac{(\rho AL)}{420}\begin{bmatrix} 140 & 0 & 0 & 70 & 0 & 0 \\ 0 & 156 & 22L & 0 & 54 & -13L \\ 0 & 22L & 4L^2 & 0 & 13L & -3L^2 \\ 70 & 0 & 0 & 140 & 0 & 0 \\ 0 & 54 & 13L & 0 & 156 & -22L \\ 0 & -13L & -3L^2 & 0 & -22L & 4L^2 \end{bmatrix}$$

$$\boldsymbol{M_\theta} = \frac{\rho I}{30L}\begin{bmatrix} 0 & 0 & 0 & 0 & 0 & 0 \\ 0 & 36 & 3L & 0 & -36 & 3L \\ 0 & 3L & 4L^2 & 0 & -3L & -L^2 \\ 0 & 0 & 0 & 0 & 0 & 0 \\ 0 & -36 & -3L & 0 & 36 & -3L \\ 0 & 3L & L^2 & 0 & -3L & 4L^2 \end{bmatrix}$$

$$\boldsymbol{M} = \boldsymbol{M_t} + \boldsymbol{M_\theta}$$

Note that, mass matrices are uncoupled for bending and axial motions.

Similar to static part, the corresponding displacement vector is

$$u = [u_1 \quad w_1 \quad w'_1 \quad u_2 \quad w_2 \quad w'_2]^T$$

Before starting the verification studies, it is deemed worthwhile to comment about the shear-locking and membrane-locking phenomena that may occur in a newly developed beam model.

Membrane locking is a phenomenon that may be seen in curved beam elements and shell elements. On the other hand, shear locking may occur in Timoshenko beam models having significant bending deformation. Since the newly developed beam element is

based on Euler-Bernoulli beam theory and the elements used in this study are straight, it is already guaranteed that shear locking and membrane locking will not occur.

CHAPTER 4

RESULTS

4.1 Verification of the Developed Formulation

In the previous chapter, the elemental stiffness and mass matrices, and force vectors are all obtained.

In order to check the accuracy of newly developed model, some comparisons are performed with the current literature. Moreover, some of the results are repeated with different number of elements. By doing so, the effect of number of elements on the accuracy of results and comparison of that effect with the current literature are both obtained within one table.

In the first comparison, the work of Park & Gao [72] is utilized. Both studies consider EBBT based on MCST. However, Park & Gao [72] solved the governing equations analytically. In the comparison, a cantilevered beam having a point load at its free end is used, as shown in Figure 4.

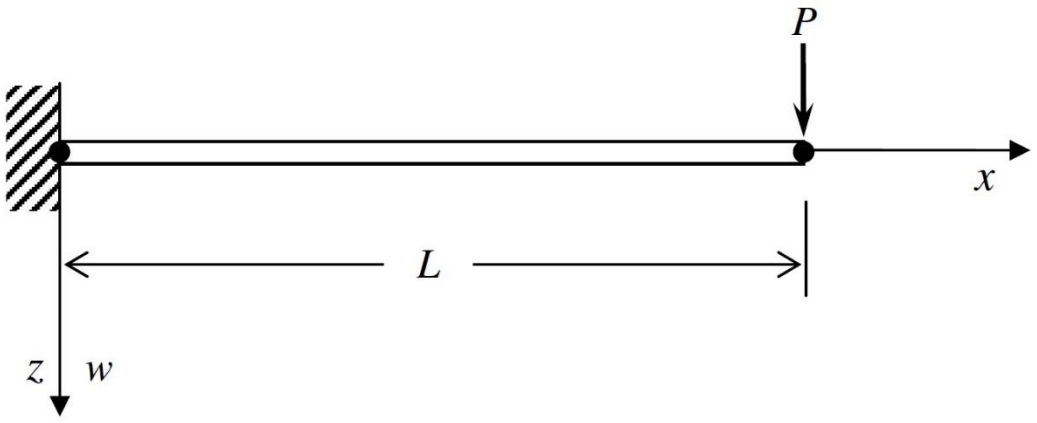

Figure 4. Cantilever beam model in [72] and [105]

The beam is a LIGA nickel foil cantilever beam with the following properties: $E = 165\ GPa$, $l = 5.6\ \mu m$, $b/h = 5$, $L = 20h$. A constant point load, $P = 1\ mN$, is applied at its free end. In the current work, the beam is discretized by 4 elements. The deflections along direction z at the four nodes are obtained (node at the fixed side is not shown). Table 3 shows the results. Moreover, the results are repeated as the height of beam cross section changes from $10\ \mu m$ to $50\ \mu m$. Furthermore, the deflection results of beams modelled with classical EBBT are also given in the comparison table in order to show the differences between the newly developed model and classical models. As it is seen, there is a good agreement between the FEM results obtained in this work and the analytical results in the work of Park & Gao [72]. It is observed that classical EBBT results are highly deviating when the height of beam (h) is comparable to length scale parameter, $l = 5.6\ \mu m$. As the height increases, classical EBBT results become similar to size dependent EBBT obtained with MCST.

Table 3. Dimensionless deflections at the nodes of a cantilevered beam under a point load at the free end

Beam Thickness	Displacement			Classical (μm)	Error % (with [72])	Deviation % (with classical)
	x-coord	Present (μm)	Park & Gao [72] (μm)			
$h = 10\ \mu m$	0.25L	13.62	13.62	33.33	0	59.14
	0.5L	49.53	49.53	121.21	0	59.14
	0.75L	100.29	100.29	245.45	0	59.14
	L	158.49	158.49	387.87	0	59.14
$h = 25\ \mu m$	0.25L	4.33	4.33	5.33	0	18.81
	0.5L	15.74	15.74	19.39	0	18.79
	0.75L	31.89	31.89	39.27	0	18.80
	L	50.39	50.39	62.06	0	18.81
$h = 50\ \mu m$	0.25L	1.26	1.26	1.33	0	5.47
	0.5L	4.58	4.58	4.85	0	5.47
	0.75L	9.28	9.28	9.82	0	5.47
	L	14.67	14.67	15.52	0	5.47

Another comparison is done with the work of Kahrobaiyan et al. [105]. In that work, researchers used MCST together with the TBT and solved numerically with FEM method. A cantilever beam is used similar to the beam shown in Figure 4. The stiffness and mass matrices of EBBT are derived in the study of Kahrobaiyan et al. [105] as a special case of TBT. Those matrices are already similar to the stiffness and mass matrices in this work. Therefore, the numerical comparison, shown in Table 4, is in very good agreement. Table 4 represents the maximum deflection of the beam. Moreover, the comparison is repeated for different number of elements (n=2, n=4, n=8). An epoxy cantilever beam is used with the following properties: $E = 144\ GPa$, $l = 17.6\ \mu m$, $h = 38\ \mu m$, $b = 0.235\ mm$, $L = 10h$. A varying point load is applied at its free end.

Table 4. Maximum deflection of a cantilevered beam under a varying point load at the free end

Load (μN)	**Deflections in the current study** (μm)			**Kahrobaiyan et al.** [105] (μm)	**Deviation % (n=4)**
	n=2	**n=4**	**n=8**		
50	0.306	0.306	0.306	0.306	0
100	0.612	0.612	0.612	0.612	0
150	0.917	0.917	0.917	0.917	0
200	1.223	1.223	1.223	1.223	0
250	1.529	1.529	1.529	1.529	0

Another comparison study is done with the work of Reddy [78]. The researcher studied functionally graded Timoshenko and Euler-Bernoulli beams with modified couple stress theory and solved the resulting equations analytically. Moreover, different from this work, von Karman nonlinearity is also included in the FG beams having power-law variation through thickness. However, researcher does not include Von-Karman nonlinearity in the results and instead of FGM, a homogenous beam is used. In the comparison, a uniform simply supported beam is used. Two different loading is used:

first a uniformly distributed load along the beam and second a point load at the mid-section. Distributed load case is shown in the Table 5.

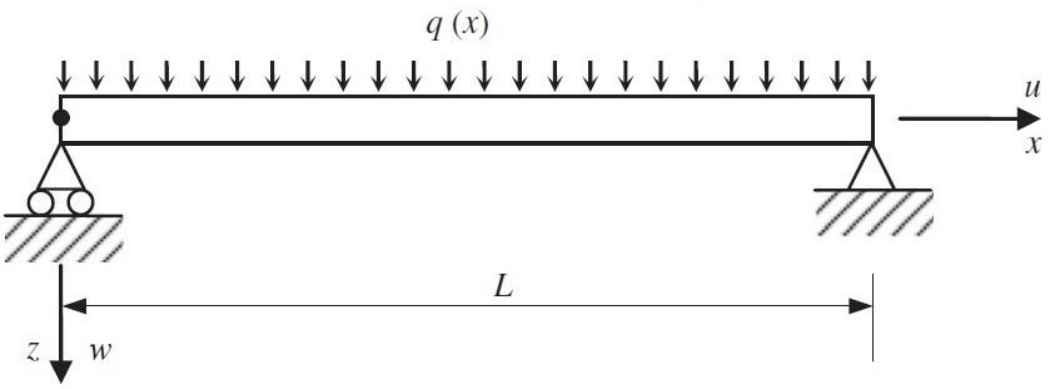

Figure 5. Simply Supported Beam Model with Distributed Load in [68] and [78]

For distributed load case, another study done by Aghazadeh [68] is also utilized for comparison purposes. In work of Reza [68], FG Timoshenko beam is solved using DQM based on SGT. The beam properties used in this work are: $E = 144\ GPa,\ h = 5 * 17.6\ \mu m,\ L = 20h,\ b = 2h$. The non-dimensonal maximum deflections are given in table 5. The deflection analysis are repeated for different l/h ratios. Note that when the FG beam is reduced to homogeneous beam, the power-law variation effect vanishes. As it can be seen, results are very similar for different l/h ratios.

Table 5. Maximum deflection of a simply supported beam under a distributed load & point load

	Distributed load $q = 1\ N/m$			**Point load** $P = qL$	
	$\bar{w} = 100 * w * \frac{E * I}{q * L^4}$			$\bar{w} = 100 * w * \frac{E * I}{P * L^3}$	
l/h	**Reddy** [78]	**Present**	**Reza** [68]	**Reddy** [78]	**Present**
0	1.3021	1.3021	1.3021	2.0833	2.0833
0.2	1.1092	1.1092	1.1092	1.7747	1.7747
0.4	0.7679	0.7679	0.7679	1.2286	1.2286
0.6	0.5076	0.5076	0.5076	0.8122	0.8122
0.8	0.3442	0.3442	0.3442	0.5508	0.5508
1	0.2435	0.2435	0.2435	0.3896	0.3896

A dynamic comparison is also carried out in this section. First three natural frequency of a simply supported beam is considered. Current work is compared with the analytical work of Reddy [78] using the same simply supported beam with the previous comparison. Moreover, classical EBBT, taken from the literature, is also utilized for comparison purposes. The results of this work and work of Reddy [78] are very similar. On the other hand, classical Euler Bernoulli beams are highly deviating as the l/h ratio increase. The results are given in Table 6, Table 7 and Table 8. The beam properties are given as: $E = 144\ GPa$, $l = 17.6\ \mu m$, $L = 20h$, $b = 2h$, $\rho = 1.22\ kg/m$

Table 6. Comparison of first natural frequency of a simply supported beam

	$\bar{w} = w * L^2 \sqrt{\frac{E * I}{\rho}}$						
l/h	**Reddy** [78]	**Present with different number of elements**			**Classical (Analytical)**	**Deviation % with Reddy** [78]	**Deviation % with Classical (n=4)**
		n=2	**n=4**	**n=8**			
0	9.86	9.91	9.87	9.87	9.87	0.1	0.0
0.2	10.68	10.74	10.70	10.69	9.87	0.1	8.3
0.4	12.84	12.90	12.86	12.85	9.87	0.1	30.2
0.6	15.79	15.87	15.81	15.81	9.87	0.1	60.2
0.8	19.18	19.27	19.2	19.20	9.87	0.1	94.5
1	22.8	22.91	22.83	22.82	9.87	0.1	131.3

Table 7. Comparison of second natural frequency of a simply supported beam

	$\bar{w} = w * L^2 \sqrt{\frac{E * I}{\rho}}$						
l/h	**Reddy** [78]	**Present with different number of elements**			**Classical (Analytical)**	**Deviation % with Reddy** [78]	**Deviation % with Classical (n=4)**
		n=2	**n=4**	**n=8**			
0	39.32	43.81	39.63	39.49	39.48	0.7	0.3
0.2	42.6	47.47	42.94	42.78	39.48	0.7	8.7
0.4	51.2	57.05	51.61	51.42	39.48	0.8	30.7
0.6	62.97	70.17	63.48	63.25	39.48	0.8	60.8
0.8	76.47	85.21	77.08	76.80	39.48	0.8	95.2
1	90.92	101.32	91.65	91.32	39.48	0.8	132.1

Table 8. Comparison of third natural frequency of a simply supported beam

	$\bar{w} = w * L^2 \sqrt{\frac{E * I}{\rho}}$						
l/h	**Reddy** [78]	**Present with different number of elements**			**Classical (Analytical)**	**Deviation % with Reddy** [78]	**Deviation % with Classical (n=4)**
		n=2	**n=4**	**n=8**			
0	88.02	110.11	90.44	88.94	88.83	2.6	1.7
0.2	95.36	119.30	97.99	96.36	88.83	2.6	10.1
0.4	114.61	143.38	117.77	115.81	88.83	2.7	32.5
0.6	140.97	176.35	144.86	142.45	88.83	2.7	63.1
0.8	171.18	214.15	175.90	172.98	88.83	2.8	98.0
1	203.54	254.62	209.15	205.68	88.83	2.8	135.4

4. 2 Static and Dynamic Analysis of a 2D Frame

In this section, static and dynamic behavior of a structure rather than a standalone beam is investigated by using the newly developed model. Moreover, the same structure is also analyzed using the commercial FEM software ABAQUS/CAE® 6.14-4. The results of this work are compared with the results of ABAQUS. In ABAQUS simulations, both Euler Bernoulli based B33 type and Timoshenko beam based B32 type elements are used.

The analyzed structure can be seen in Figure 6:

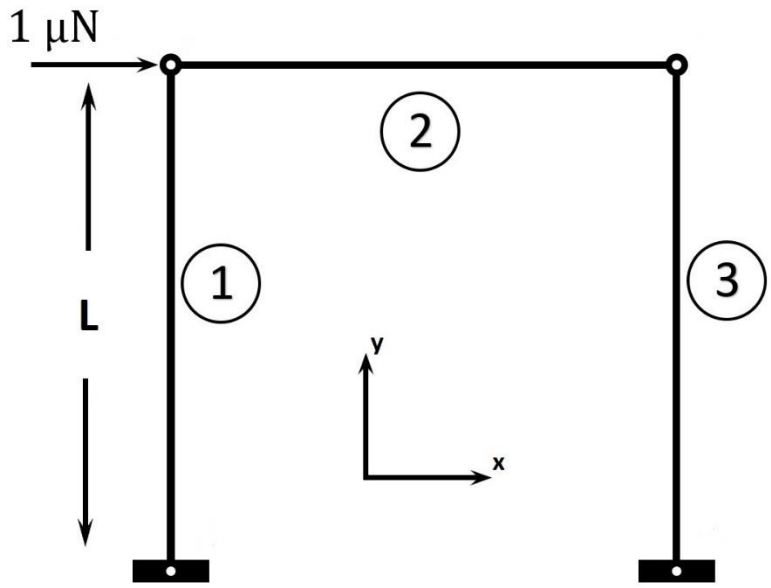

Figure 6. A structure with three beams welded to each other and ground

The structure consists of three identical beams, having the same material and dimensions. They are welded to each other and to the ground. A $1\mu N$ force, acts horizontally at the upper left corner, as shown in the figure. The properties of beams are given below:

- Material: Epoxy
- Elastic modulus (E): $1440\ MPa$
- Poisson's ratio (ϑ): 0.38
- Density (ρ): $1.22 * 10^{-9}\ ton/mm^3$
- Material length scale parameter: (l): $17.6\ \mu N$
- Height of the beam at cross section (h): $35.2\ \mu N, 17.6\ \mu N, 8.8\ \mu N$
- Width of the beam at cross section (b): $35.2\ \mu N, 17.6\ \mu N, 8.8\ \mu N$
- Length of the beam (L): $0.352\ mm$

There are three different height and width values of the beams. Because, the comparison is repeated three times. As the height and width of the beam become smaller, the results of the current study is expected to differ much more from the results of ABAQUS using classical theories.

Note that the mesh used in ABAQUS is generated both using Euler-Bernoulli beam theory and Timoshenko beam theory. Therefore, the results of this work is compared to both classical Euler-Bernoulli and classical Timoshenko theories. Moreover, the study is repeated for different number of elements, n=1, n=2, n=4 for each beam.

4.2.1 Static Results

Table 9 shows the deflection values in *x* direction of the point where the force is applied.

Table 9. Deflection values of the force applied point along x-direction

Height of beam (μm)	Number of elements	DEFLECTION RESULTS (mm)				Deviation (%) between 1&2
		ABAQUS Euler	ABAQUS Timoshenko	1 Current (l=0)	2 Current	
35.2	1	0.0142	0.0147	0.0142	0.00687	51.6
	2	0.0142	0.0147	0.0142	0.00687	51.6
	4	0.0142	0.0147	0.0142	0.00687	51.6
17.6	1	0.226	0.228	0.226	0.0427	81.1
	2	0.226	0.228	0.226	0.0427	81.1
	4	0.226	0.228	0.226	0.0427	81.1
8.8	1	3.609	3.617	3.61	0.198	94.5
	2	3.609	3.617	3.61	0.198	94.5
	4	3.609	3.617	3.61	0.198	94.5

The newly developed model is used by setting the length scale parameter both to zero and its real value in the current model. Therefore, current model is utilized both in classical and in higher order continuum modes. The results indicate that outcomes based on current model are in good agreement with the outcomes of ABAQUS in both Euler and Timoshenko beam theories if the length scale parameter is taken as zero. However, when the effect of length scale parameter is included in the current study, the results deviate. The deflections when size effect is included are smaller than the others, which means the structure behaves stiffer. This conclusion is consistent as discussed in previous sections. Moreover, as the beam becomes smaller and smaller, the amount of deviation increases relatively. The last column shows the percent deviation. As the beam height decreases, percent error increases from 50s to 90s. Size effects are much higher in smaller beams, when the beam dimensions are comparable with the length scale parameter.

Different element numbers do not have a significant effect on the results. The solution is the same with the exact solution regardless of mesh size. This is due to the fact that the order of polynomial of exact solution and interpolation functions are the same [114].

Moreover, since the ratio between length and height is high enough (slenderness ratio), the Euler beam theory and Timoshenko beam theory give similar results. Timoshenko beam theory gives slightly higher deflection results since transverse shear deformation is included in Timoshenko beam theory, which causes less stiffness with respect to Euler Bernoulli beams.

4.2.2 Dynamic Results

The dynamic analyses are carried out on the same structure by eliminating the force. Table 10, Table 11 and Table 12 show the first, second and third natural frequencies of the structure. ABAQUS is utilized similar to the static results by implementing both Euler Bernoulli and Timoshenko beam theories. Current work is also used by taking the length scale parameter both zero and its real value. Note that in the examined structure natural frequencies always correspond to the deformation mode.

Table 10. First natural frequency of the structure

Height of beam (μm)	Number of elements	FIRST NATURAL FREQUENCY (KHz)				Deviation (%) between 1&2
		ABAQUS Euler	ABAQUS Timoshenko	1 Current (l=0)	2 Current	
35.2	1	45.5	45.5	45.8	65.7	43.4
	2	45.4	44.7	45.3	65.3	44.2
	4	45.4	44.6	45.3	65.3	44.2
17.6	1	22.8	23	22.8	52.5	130.3
	2	22.7	22.6	22.7	52.1	129.5
	4	22.7	22.6	22.7	52.4	130.8
8.8	1	11.4	11.6	11.4	48.7	327.2
	2	11.4	11.4	11.3	48.5	329.2
	4	11.4	11.4	11.4	48.6	326.3

Table 11. Second natural frequency of the structure

Height of beam (μm)	Number of elements	SECOND NATURAL FREQUENCY (KHz)				Deviation (%) between 1&2
		ABAQUS Euler	ABAQUS Timoshenko	1 Current (l=0)	2 Current	
35.2	1	209.9	204.7	209.5	291.1	38.9
	2	177.1	174	176	250	42.0
	4	176.1	171.2	175.3	247.6	41.2
17.6	1	107.3	107.9	106.5	238.5	123.9
	2	89.9	90.3	89.7	203	126.3
	4	89.4	88.7	89.2	202	126.5
8.8	1	53.9	54.7	53.6	222.6	315.3
	2	45.1	45.6	45.1	189	319.1
	4	44.8	44.9	44.8	188.1	319.9

Table 12. Third natural frequency of the structure

Height of beam (mm)	Number of elements	THIRD NATURAL FREQUENCY (KHz)				Deviation (%) between 1&2
		ABAQUS Euler	ABAQUS Timoshenko	1 Current (l=0)	2 Current	
35.2	1	482.3	463.2	457.5	625.4	36.7
	2	295.5	290.2	293	423	44.4
	4	292.1	278	290.2	418	44.0
17.6	1	245.2	262.5	230.7	525.4	127.7
	2	148	151.6	148	341	130.4
	4	146.3	144.7	146.1	337	130.7
8.8	1	123	136.1	115.7	490.4	323.9
	2	74	76.6	73.9	316	327.6
	4	73.2	73.6	73.2	313	327.6

The results show that, in general, current work is in good agreement with the results obtained from ABAQUS. Natural frequencies of the structure obtained by considering small-scale effects are higher than the natural frequencies computed by using other methods. It can be inferred that, similar to the static case, structure behaves stiffer under small-scale effects. Moreover, stiffness of the structure increases relatively, as the height of beam decreases. Because, small-scale effects become more dominant as the dimensions of beam become smaller. This can be observed from the percent errors shown in the last column.

The mode shapes generated by classical theories and current work are similar. In the Figure 7, mode shape of the structure obtained from ABAQUS can be seen for the first, second and third natural frequencies.

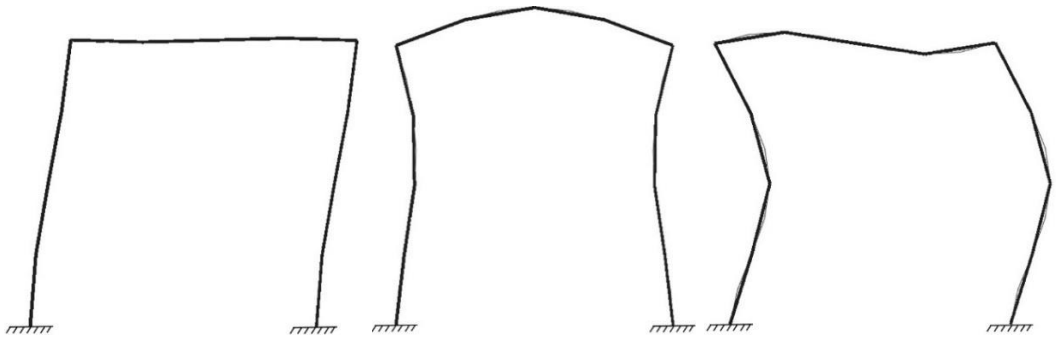

Figure 7. First three mode shapes of the structure

The developed code which is used to generate the presented results for the structure is given in the Appendix A.

4.3 Mesh Stiffness Calculation for Spur Gears

4.3.1 Introduction

Gears are the most frequently used machine elements in transmission systems. Although the gears have been used for ages in very different areas and applications, still many studies are being done to understand the operational behavior of gears. One of the most important topics of these kind of studies is the mesh stiffness calculation of a gear pair or a system having several gear pairs in action at the same time.

Gears are machine elements having a stiff (firm) inner part, namely the gear hub which can be likened to a strong foundation. There are teeth located circumferentially like cantilever beams on this foundation. When the teeth of mating gears are in contact, the load is transmitted from one teeth to another. This load transmitting gear pair region is called gear mesh. The contact behavior of the gear mesh is closely related with the mesh

stiffness. In the literature, there are some studies such as [115]–[119] to determine the correct mesh stiffness of a gear pair in macro scale. Although micro gears are popular machine elements used in MEMS due to some advantages such as higher operating speeds, low cost in serial production [120], comprehensive studies about the mesh stiffness of micro-gears does not exist in the literature. In order to understand strength, deformation mechanism and dynamic behavior of micro-gear pairs, mesh stiffness of micro gears is believed to be an important field that should be investigated. For instance, Figure 8 shows a view of the microengine output gear and two additional driven gears [121]. The gears have 50 μm tip diameter and 2.5 μm facewidth.

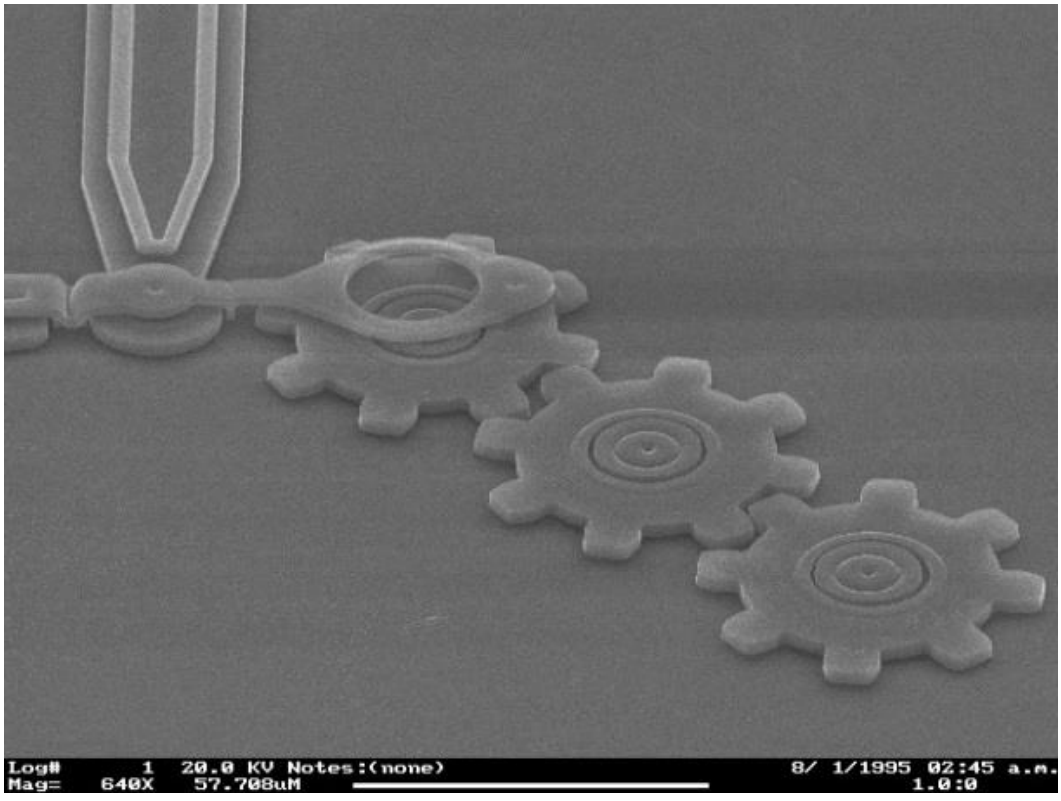

Figure 8. An example of micro gear train

In this section of the thesis, a mesh stiffness calculation method for macro scale gears will be demonstrated first. Obtained results will be compared with the results in the literature. After the mesh stiffness calculation is verified for macro gears, the procedure will be applied to micro scale gears using the newly developed beam finite elements which have a length scale parameter for micro-size applications. This section will be concluded with discussions regarding the behavior of gears in micro scale.

4.3.2 Calculation

There are different types of mesh stiffness calculations in the literature. Basically, the methods can be divided into three groups: experimental studies, analytical studies and numerical studies.

Due to the challenges of doing experiments in order to study the gear mesh, experimental studies are not very common in the literature. Moreover, analytical studies are applicable mostly to the simple geometries and to the specific gear pairs. Therefore, analytical studies are limited after some point in the mesh stiffness calculations. On the other hand, due to the applicability to any kind of problems and attainability of highly accurate results, numerical studies are relatively more popular than the experimental and analytical studies.

Various researchers have used different types of numerical methods in the calculation of mesh stiffness. These are thin slice method (1D), finite strip method (1.5D), finite quasi-prism method (2.5D), finite element method (1D, 2D or 3D).

In this study, 1D finite element method is utilized.

4.3.3 Representation of Tooth Geometry and Loading

For the mesh stiffness calculation of a gear-pair, firstly tooth geometry is generated, then load and boundary conditions are applied accordingly. By using corresponding surface equations [122], an involute profile of a spur gear is generated. A third degree polynomial is fitted to the coordinates of obtained involute profile. The polynomial equation takes the radial distance measured from the dedendum circle and returns back the thickness at that specific height, which enables one to obtain the tooth thickness value of involute profile at any diameter between dedendum and addendum diameters of the gear.

After these preparatory steps, the involute profile can now be successfully divided into required number of finite elements. A representative figure of how involute profile is divided into elements is given in Figure 9.

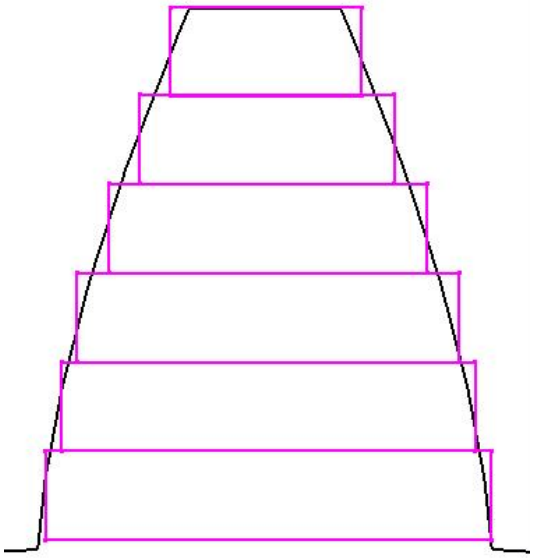

Figure 9. Involute profile of spur gear and finite element representation

In Figure 10, a typical gear tooth loading is given.

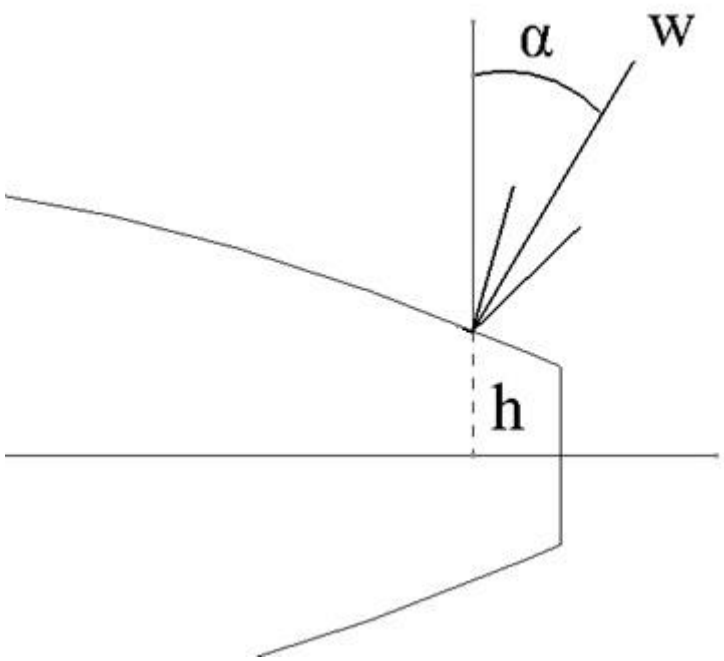

Figure 10. Loading of a typical spur gear tooth

The load w is applied perpendicular to the tooth surface along the tooth profile in contact. The resulting components of the force in the horizontal and vertical directions are given as,

$$w_h = w * \sin\alpha$$

$$w_v = w * \cos\alpha$$

where, w_h is the horizontal (radial) component and w_v is the vertical (tangential) component. Horizontal force w_h causes a moment about the center of the gear foundation given as,

$$M = w_h * h$$

The main deformation mechanisms due to these components are the displacement and rotation caused by the vertical force w_v and the rotation caused by moment M. Equivalent force system acting on tooth axis is shown in Figure 11.

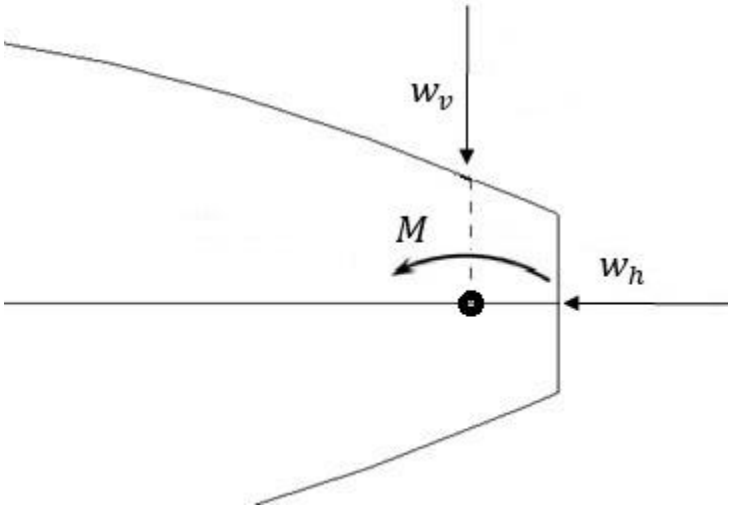

Figure 11. Equivalent loading components of a typical gear tooth

Note that, the axial deformation due to horizontal force component , w_h, is neglected since the contribution of that component to deformation along the vertical direction is relatively small.

The general deformation mechanism of a gear tooth under contact load is briefly explained above. In the literature, there are different ways of simulating the deformation mechanism of gear tooth. The most accurate way of reperesenting the deformation mechanism of gears is the simulating the gears and teeth as solid elements. There are

studies in the literature that use solid elements in micro scale, such as [123]. However, using solid elements for micro gear pairs to calculate the mesh stiffness can be pretty cumborsome. In order to have a practical method to get mesh stiffness of micro gears correct and accurate enough, Euler-Bernoulli and Timoshenko Beam elements can be applied instead of solid elements. Therefore, in this work, the mesh stiffness of a spur gear pair is estimated by using cantilever beams having loads at their end sections [124]. The simulation procedure can be seen in Figure 12.

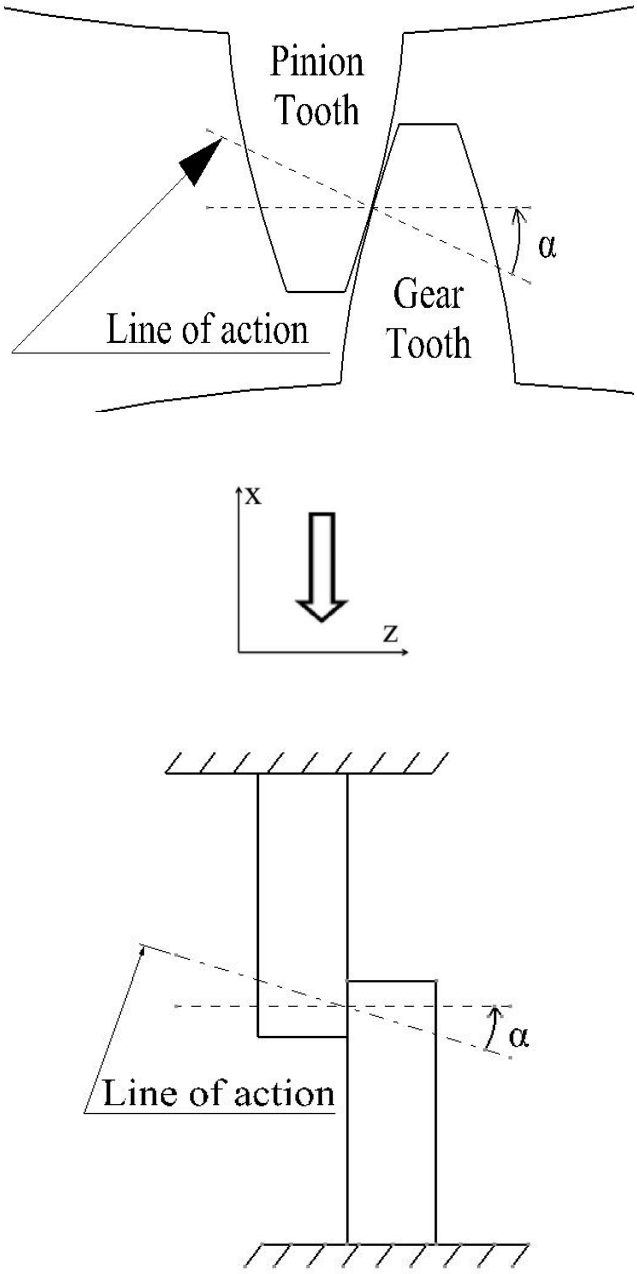

Figure 12. Tooth pair in contact and cantilever representation of a pair

Figure 12 shows the cantilever representation of a pair that does not take into account the effect of foundation (gear rim thickness) because gear is fixed from the base circle. Also, the variation of the tooth thickness along the profile of the spur-gear in not considered. In the current study, the effect of foundation is also not taken into account. However, as it can be seen on Figure 9, variation of the tooth thickness along the profile of spur gear is considered. In order to obtain the stiffness of a spur gear, according to Castigliano's second theorem, the force components are applied to each determined contact point separately and then the deflection of "force application point" is recorded along the direction of force. The finite element discretization is done accordingly to make determined contact points coincident with the finite element node locations intentionally.

It is important to note that the applied force w_v and moment M are assumed to contribute to the deformation of the tooth surface along the z-direction. In reality, main deformation of the tooth occurs along the line of action. In order to further converge to the reality, the displacements in z direction should be converted to the displacement along the line of action. For this, the displacements in the z direction are divided by the cosines of angle between direction of force and surface normal following Mathur et. al. [118] (angle α on Figure 12). After converting the direction into line of action, obtained deflections from model are converted to stiffness using the equation below,

$$K = \frac{F}{U}$$

The unit of K is N/mm. Note that the same procedure is repeated for a number of sample contact points on one tooth as the load application (contact) point moves on the tooth surface while the contact point moves along the line of action. In order to obtain the mesh stiffness, similar procedures are done for the conjugate gear tooth in contact. Then the mesh stiffness of the gear pair is obtained as shown below,

$$K_{mesh} = \left[\frac{1}{K_1} + \frac{1}{K_2}\right]^{-1}$$

Here, K_1 and K_2 are the stiffnesses of gear tooth 1 and gear tooth 2, respectively. K_{mesh} is the mesh stiffness of the contacting pair. As given in the literature, the obtained mesh stiffness is divided by facewidth. Then the result is further divided to a thousand to have the unit $N/(mm * \mu m)$ as done in the works of the other researchers.

It is important to note that, the obtained stiffness is the mesh stiffness of only one pair. According to value of the contact ratio, which is related with the number of pairs in contact at the same time, mesh stiffness should be modified accordingly.

To sum up the procedure, Figure 9 is updated and Figure 13 is generated to clearly demonstrate the applied load and obtained displacements.

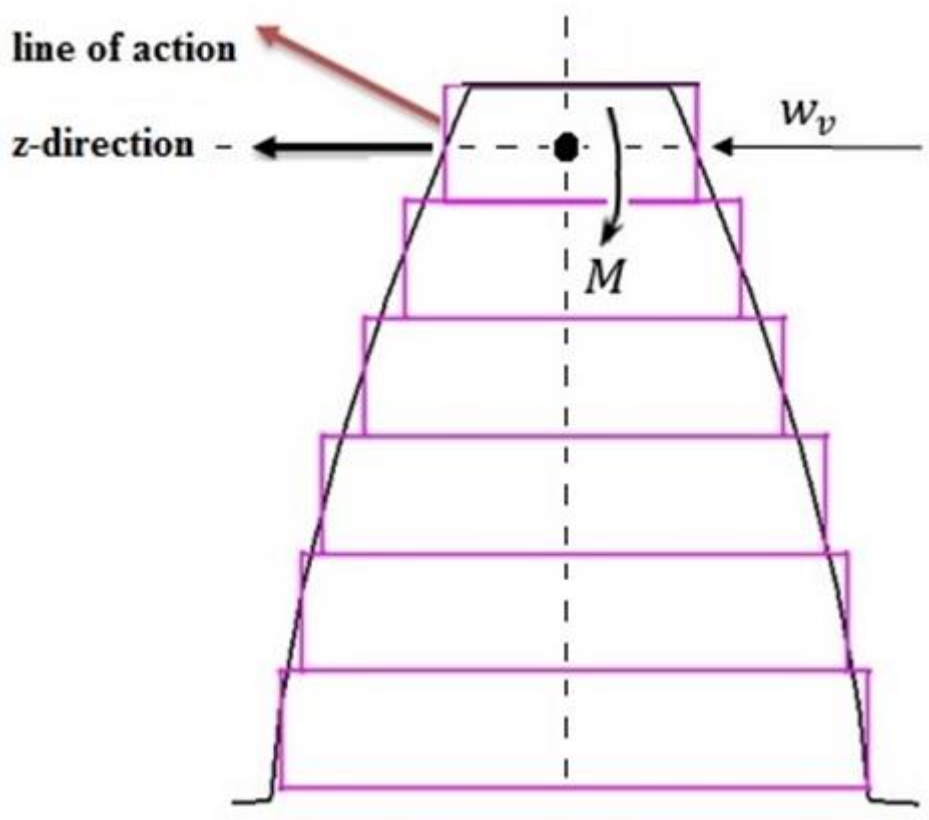

Figure 13. Applied loads and direction of displacement

In the Figure 13, black arrow on the left shows the obtained displacements due to the applied loads. Red arrow shows the displacement along the line of action which is generated using the displacements along the z direction. Note that the angle between red and black arrow changes as the point goes from ti to the base.

4.3.4 Verification

In order to check the accuracy of the developed model for the mesh stiffness of micro-gears, a verification study will be carried out with macro gears existing in the literature. Chang et al. [119] obtained the mesh stiffness of a gear pair by utilizing finite element

method and contact analysis of elastic bodies. In the work of Chang et al. [119], the obtained method is also compared with methods called Cai Method & Kuang method. Those results are also given in this work. Moreover, a mean value of mesh stiffness is obtained for three different methods together with the mean stiffness value obtained from international standard ISO6336-1, "Calculation of load capacity of spur and helical gears" [125]. Since other methods use $300\ N/mm$ for the tangential force per unit width, same force is also used in the current study.

Macro Gear properties:

- Number of teeth: 65/65
- Module (mm): 3
- Pressure angle: 20°
- Helix angle: 0
- Facewidth (mm): 60
- Addendum coefficient: 1
- Modulus of elasticity (GPa): 207
- Contact ratio:1.8
- Length of action (mm): 15.9

In order to estimate the contact region of gear pairs correctly, KissSoft 2013B is utilized. The contact ratio of the gear pair is found as 1.8. Moreover, from KissSoft, the range of circular diameters at which single pair of tooth is in contact and the range of circular diameters at which two pairs of teeth are in contact are obtained. Using this knowledge, the most suitable number of elements to be used to approximate the involute profile of tooth is calculated. In this calculation, node positions are arranged such that the circular diameters where the beginning of contact of two pair, beginning of contact of one pair and end of contact of one pair is tried to be matched with the node positions properly. Note that, in reality, as the contact moves from gear base towards gear tip, distance travelled on tooth increases at the same time interval since the circular speed is higher at

tip of gears if the rotational velocity of gears is kept constant. This causes sliding of one gear over the other. In our calculations, the sliding velocity of gears is considered as zero.

Considering all those preparatory steps, the involute of gear profile is represented with 32 elements. The contact starts at node 13. Until node 21, two gear pair are in contact. Then, from nodes 21 to 25, one gear pair is in contact. Afterwards, again two pairs are meshed with each other. Figure 14 shows the teeth pair node numbering and the overlapping nodes of each tooth.

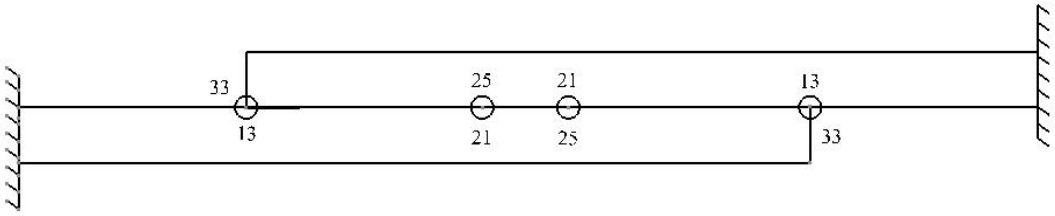

Figure 14. Spur gear pair node numbering

In the current work, Euler-Bernoulli beam model (EBT) is used. The main assumption of Euler-Bernoulli beam model is that plane cross sections perpendicular to the beam axis remain plane and perpendicular to the neutral axis as the beam deforms. On the other hand, in Timoshenko beam model (TBT), a rotation exists between cross section and neutral axis. Shear deformation is the reason of this rotation, which is not included in Euler-Bernoulli beams. Therefore, Euler-Bernoulli beam is stiffer than Timoshenko beam. However, if the ratio of the length of the beam to the thickness of beam is large enough, two different beam models give same results. Therefore, as a rule, it is better to use Timoshenko beam model for shorter and thicker beams. Therefore, in the comparison of current work with the work in the literature, for further understanding of the mechanism of mesh stiffness of a gear pair, the developed stiffness matrices in the current study are used together with the stiffness matrices developed for micro beams using Timoshenko beam model in the work of Dehrouyeh-Semnani & Bahrami [110].

The results obtained in Chang et al. [119] are given in Figure 15 as mesh stiffness versus normalized time with respect to mesh cycle after which the cycle repeats itself. The mesh stiffness equation used in that work given below:

$$K_w = \sum_{i=1}^{n} k_i = \sum_{i=1}^{n} \frac{F_i}{\delta - \varepsilon_i}$$

Where k_i is the stiffness of each contact pair, ε_i is the initial separation distance between contact points, δ is the static transmission error and F_i is the contact force at contact point i. The obtained result is divided by the facewidth and represented. The time varying mesh stiffness over mesh cycle is calculated by computing the stiffness at different moments.

Moreover, by using the same gear and load data, KissSoft is also used to analyze the mesh stiffness. KissSoft uses Weber/Banaschek formulations to estimate the mesh stiffness. It takes into account the tooth deformation, gear body deformation and flattening due to Hertzian pressure. Figure 16 shows the result of mesh stiffness obtained from KissSoft. Figure 16 also shows the mesh stiffness obtained with the current work using two different methods, both Euler-Bernoulli Beams and Timoshenko beams.

Note that the normalized time axis of both of the figures, Figure 15 and Figure 16, ranged between 0 and 1. Because, after one double mesh and one single mesh region, the graph again continues with double mesh region and repeats itself.

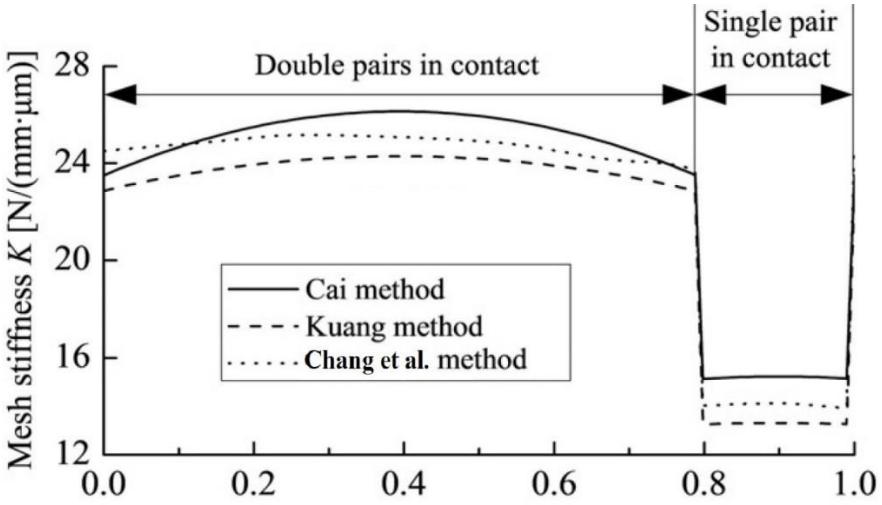

Figure 15. Mesh Stiffness Curve of Different methods [119]

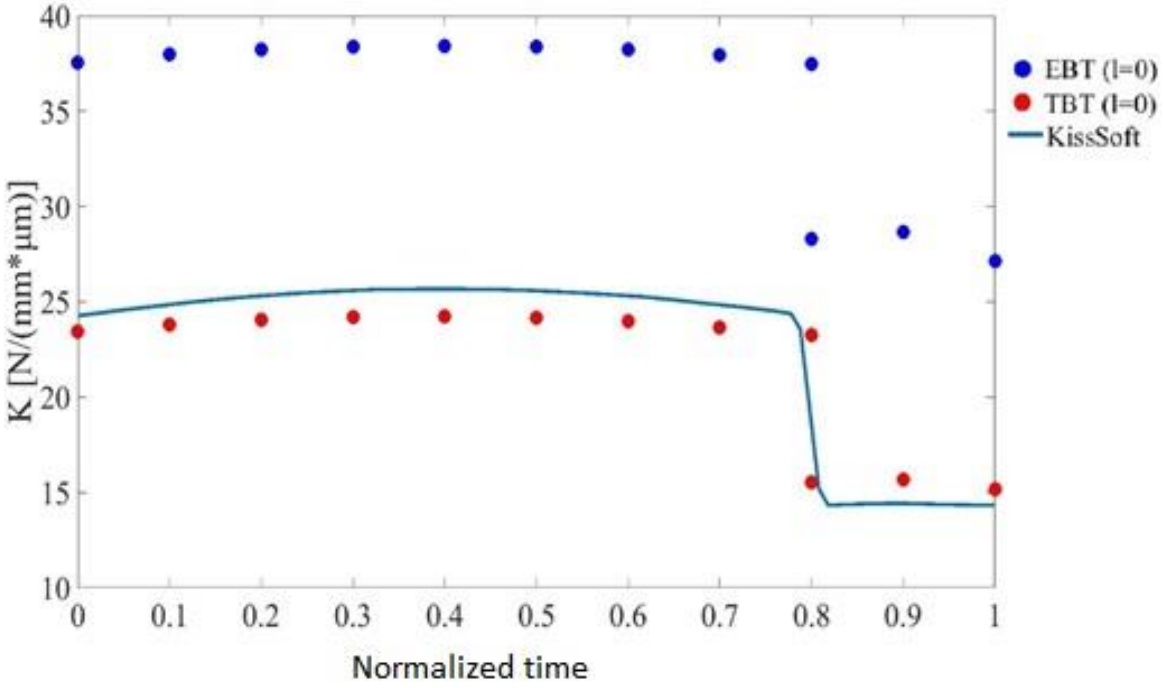

Figure 16. Mesh Stiffness calculated by KissSoft and Current Study

In Figure 15, it is seen that for all three different studies, approximately, double mesh stiffness region has its maximum about 25 $N/(mm * \mu m)$ and single pair region has its maximum about 14 $N/(mm * \mu m)$. Similar results are obtained from KissSoft as seen in Figure 16.

In the current work, for the calculation using Euler-Bernoulli beam model, double mesh stiffness region has its maximum about 38 $N/(mm * \mu m)$ and single pair region has its maximum about 28 $N/(mm * \mu m)$. On the other hand, for the calculation using Timoshenko beam model, double mesh stiffness region has its maxiumum about 24 $N/(mm * \mu m)$ and single pair region has its maximum about 16 $N/(mm * \mu m)$.

For the given parameters, mesh stiffness curves generated in the work Chang et al. [119] and KissSoft show similar results. Although there are small differences between them, the general trend of curves are very similar. The current work is also very similar to those works in terms of the trend of curves in the plot. However, the results are higher. Also, the stiffness values obtained by using Timoshenko beam model are very similar to those works.

The mean mesh stiffness values for different mehods together with current work are also given in the Table 13. Note that for mean mesh stiffness values, ISO6336-1 [125] is also utilized and compared with current work.

Table 13. Mean values of mesh stiffness of different methods

Method	**Mean Mesh Stiffness [N/(mm*µm)]**
ISO6336	23.25
Cai	23.25
Kuang	21.69
Liu & Wu	22.68
Current with Euler Bernolli	36.06
Current with Timoshenko	22.69

Mean stiffness value of the current work using Timoshenko Beam Theory (TBT) lies between the results of the four different methods as it can be seen in Table 13. However, the mesh stiffness results obtained by using Euler Bernoulli beam theory (EBT) are relatively higher than all the other results. This means that the gear mesh modelled with Euler-Bernoulli beam behaves stiffer than any of the other models. This is an expected behavior of the beam, because, the involute profile of tooth is modelled with beams that are short and thick. If the shear deformation is not considered for those types of beams, as assumed in Euler-Bernoulli beam model, the beams behave stiffer. Since the Timoshenko beam model considers shear deformation, the beam models of this kind deforms more than the Euler-Bernoulli beams. More deformation means less stiffness. Therefore, the result itself is consistent.

The results of current work are all obtained without using length scale parameter values. For all results, length scale parameter is taken as zero. Because, for the selected material there is no study that determines the length scale parameter in the literature. However, considering the verifications studies in previous chapters, it is believed that for the given tooth geometry in macro scale, using length scale parameter will not make any difference in results.

Moreover, there are some error sources in the current model.

The first source is that when two gears get in contact, the tooth deflection is affected by the foundation of gear. Together with teeth, foundation of gear also deflects, which affects overall stiffness of gear. In our model, the foundation is neglected and gear is modeled as a cantilever beam by fixing it from base radius as if it has a rigid foundation. This eventually may cause higher stiffness results in the current study. However, since the gear foundation is very strong when compared with the tooth section, the results does not show significant deviation. Therefore, it is concluded that neglecting foundation of gear is a reasonable assumption.

Another error source is the effect of applied force. In our model, the mesh stiffness is dependent upon geometry of gear and independent of applied force. However, in reality, as the force increases mesh stiffness of gear pair also increases. This is basically the result of deflection on tooth, as the force changes on gear. As the load is increased, deformation and therefore contact ratio increases. That is why, at low spesific loadings, stiffness is dependent upon the applied load [125], which provides larger resistance against the applied load or torque. This phenomenon will be again discussed later on this.

Another error source, as discussed previously, is that sliding velocity of gears is taken as zero. This assumption is originated from the node to node interaction requirement of finite element method. If sliding velocity is included in the current work, the length of double gear mesh region of two pairs will not be same. For instance, in this specific example, nodes 13-21 and 25-33 are the regions where double mesh is in contact as shown in Figure 14. In the current cantilevered beam model, distance between nodes 13 & 21 is same with the distance between nodes 25 & 33. Therefore, each node in 13-21 region of one gear has a counter meshing node at 25-33 at the conjugate gear and vice versa. However, since as the circular diameter increases, circumferential velocity of gear increases if angular velocity is kept constant. Therefore, mesh travels more distance as it goes from base to tip diameter of gear, which causes a sliding motion between gears. Practically, this should have resulted with the fact that 13-21 region is shorter than 25-33 region. Since the current work uses equally distanced nodes and has a node-to-node

interaction at each step, this representation is not possible. In Figure 16, it can be seen that, the trend of curve is little bit distorted at the end sections of the single mesh pair, for both Euler-Bernoulli and Timoshenko beam model. This is basically due to the assumption of zero sliding velocity.

4.3.5 Micro Gear Mesh Stiffness

In this section, using two different tooth geometries in micro scale, mesh stiffness calculations will be done. For both gears, epoxy is used as a material which has a known length scale parameter.

Same procedure explained in the previous section is also followed in this section; therefore, preparatory steps will not be explained in detail. Length scale parameter is taken as both zero and real value for epoxy material. Two different results are obtained for two different length scale parameter values. Moreover, results are calculated using both Euler-Bernoulli and Timoshenko beam models. Although, Kisssoft does not have a capability of capturing size effects for small-scale gears, still it is also used to get mesh stiffness value of the micro gears in order to compare the results with the current study. Note that the tangential force, for the 2 different case studies given below, are arranged such that the contact ratio of the system is similar to the contact ratio of the system used in the verification study, which assures that the current case study follows exactly the same procedure as it is done in the verification study.

Gear geometries for gear pair 1:

- Number of teeth: 59/59
- Module (mm): 0.05
- Pressure angle: 20°
- Helix angle: 0
- Facewidth (mm): 1
- Addendum coefficient: 1
- Modulus of elasticity (GPa): 1.44
- Length of action (mm): 0.263
- Contact ratio:1.8
- Length scale Parameter (mm): 0.0176

The mesh stiffness results for the gear pair 1 are given in Figure 17.

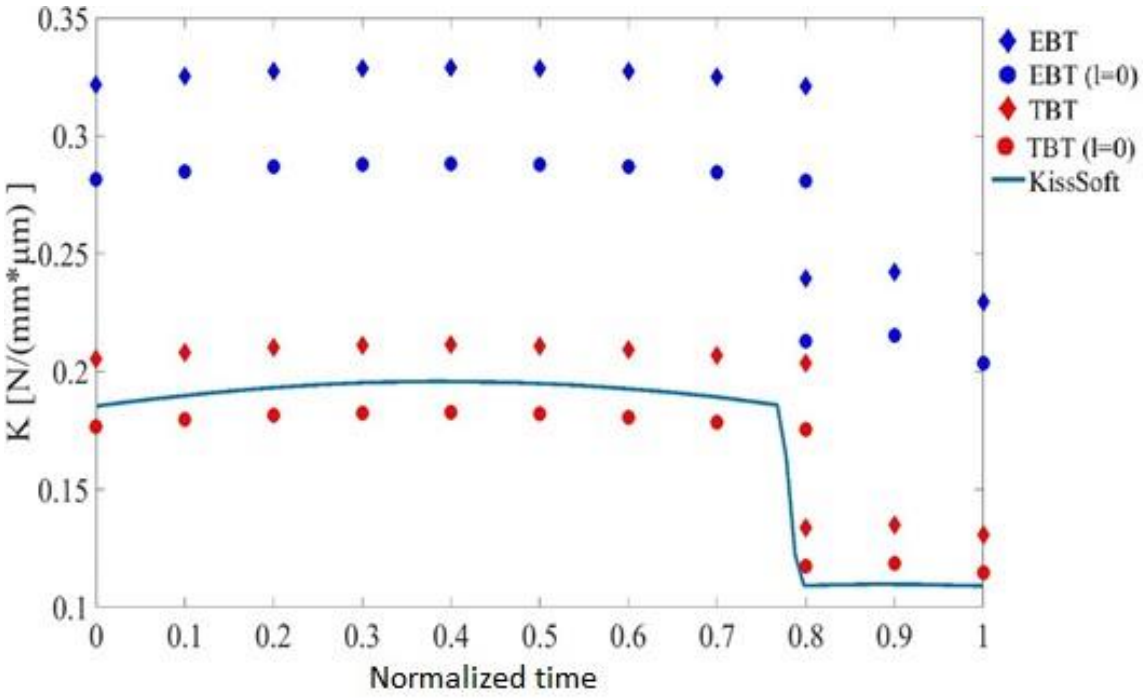

Figure 17. Mesh Stiffness results of KISSSOFT and Current Study for 0.05 module

Before starting the discussion of the results, in order to understand the effect of length scale parameter as the size of micro gears changes, mesh stiffness of a second micro-gear, which is smaller than the first micro gear, is also obtained.

Gear geometries for gear pair 2:

- Number of teeth: 59/59
- Module (mm): 0.01
- Pressure angle: 20°
- Helix angle: 0
- Facewidth (mm): 1
- Addendum coefficient: 1

- Modulus of elasticity (GPa): 1.44
- Length of action (mm): 0.053
- Contact ratio:1.8
- Length scale Parameter (mm): 0.0176

Figure 18 shows the results of KissSoft and current study for gear pair 2.

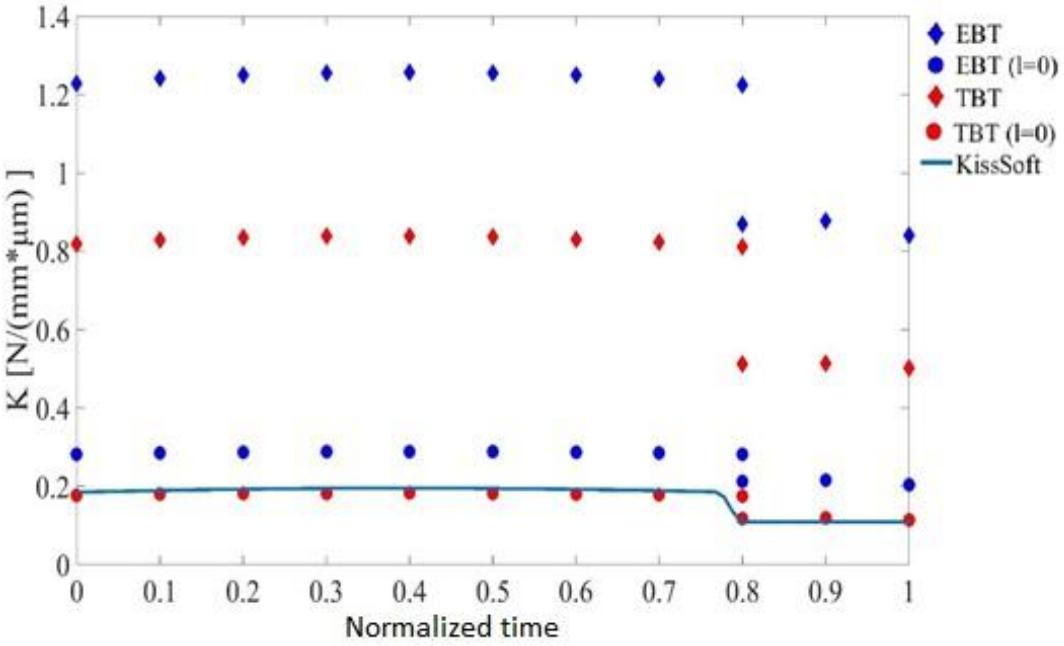

Figure 18. Mesh Stiffness results of KISSSOFT and Current Study for 0.01 module

Furthermore, Table 14 shows the mean mesh stiffness values of current work.

Table 14. Mean mesh stiffness values of gear pairs for different beam theories

	Method	Mean Mesh Stiffness [N/(mm*µm)]	% Difference between two length scale paramater values
Gear Pair 1	EBT (l=0)	0.27	12.90
	EBT	0.31	
	TBT (l=0)	0.17	10.53
	TBT	0.19	
Gear Pair 2	EBT (l=0)	0.27	76.72
	EBT	1.16	
	TBT (l=0)	0.17	60.00
	TBT	0.77	

From Figure 17 it can be seen that KissSoft and current work based on Timoshenko beam theory is very similar both at double pair contact regions and single pair contact region if the length scale factor is taken as zero. The current work based on Euler Bernoulli beam theory shows higher mesh stiffness results. If the length scale parameter in the current work is set to its real value for epoxy material, the results start to deviate from the results obtained from KissSoft, which is due to the fact that length scale parameter are comparable with the dimensions of tooth at these sizes. Therefore, the classical continuum theories start to deviate from reality. This conclusion can also be drawn from Figure 18. However, different than the Figure 17, deviations in the results seen on Figure 18 are much higher, because, the gears in pair 2 have smaller teeth than the gears in pair 1. Thus, size effects becomes much more prominent for the gears in pair 2.

Moreover, the mesh stiffness values including size effect are higher, which means that smaller gears deforms less than their expected values in classical continuum theories. It can be said that, in general, tooth profile considering the micro effects behaves stiffer. As the micro gear becomes smaller, the stiffening effect increases. Therefore, the differences between classical and non-classical results on Figure 18 are much higher than the results on Figure 17. This fact can also be seen on Table 14. The percent difference values on Table 14 are higher for gear pair 2 because gear pair 2 has smaller gears than the gears in gear pair 1. This concludes that smaller gear behaves stiffer.

CHAPTER 5

CONCLUSION AND FUTURE WORK

It is known that the classical continuum theories used to describe the general behavior of beams and structures built-up with beams are highly deviating in the micro levels. An additional parameter called length scale parameter should be introduced to the classical continuum theories in order to capture the correct behaviors of beams in micro scale. This parameter has a different value for each material and determined by experiments. If the beam dimensions are so small that they are comparable with the length scale parameter, then size effects are observed in the mechanical behavior of the beam. The classical continuum theories which do not include any length scale parameters are not able to capture the size effect and thus they are deviating from the reality as the beam dimensions become smaller and smaller. However, the higher order continuum theories includes the length scale parameter and it is shown that they are very good at reflecting the real behavior of micro beams and structures that are made from micro beams.

In this thesis, a size dependent finite element is developed for micro beams using modified couple stress theory together with Euler-Bernoulli beam theory. The Galerkin method is employed and stiffness and mass matrices are generated for the new beam element. A MATLAB code is also prepared to implement this element. By doing so it is believed that a convenient tool to analyze structures made up of beams in micro scale. After verification and comparison studies of the newly developed element, two original case studies are carried out.

The first case study is the static and dynamic analysis of a frame. For this case study, three micro-beams, welded to each other and to a rigid foundation, are used and

deflections under force and natural frequencies are obtained and compared with the classical methods. Although the mode shapes obtained in this work are similar to the mode shapes that are generated by classical theories, it is observed that the static and free vibration responses of the micro structure are relatively stiffer. In this case study, unlike the works in the literature, the newly developed model for micro-beam is utilized on a 2D frame structure instead of simple beam solutions. It can be inferred that, the application of the new model to the structure is consistent and successful because of the good agreement between the results of current work and results obtained from the ABAQUS.

The second case study is related with the mesh stiffness of micro gears. A FEM based procedure to obtain the mesh stiffness of a gear pair is introduced. The verification and comparison studies of the method are carried out for macro gears to be compared with already existing works in the literature. Then, the verified procedure is applied to two different micro gear pairs and the differences between mesh stiffness of macro and micro scales are discussed. It is again observed that when the gears are small enough, size effect causes a relatively stiff behavior. It is believed that the mesh stiffness calculation part of this study is a novel contribution to the literature. Although micro gears are becoming more and more popular in the industry, to the best of author's knowledge, there are no studies considering the mesh stiffness of micro gears including size effects. The current work showed that, the standard mesh stiffness calculation tools are deviating in micro scale.

As a future work, the obtained stiffness and mass matrices can be implemented to the FEM software that have user interface plugins which enables users to introduce their own elements from outside. By doing so, size effect phenomenon can be implemented to the existing FEM software and their powerful interfaces and calculations for complicated structures can be utilized.

In this work, mesh stiffness values of spur gear pairs are investigated. The study can be expanded towards different types of gears such as helical gears, bevel gears etc. in micro scale in the future.

REFERENCES

[1] "Introduction and application areas for MEMS." [Online]. Available: http://www.eeherald.com/section/design-guide/mems_application_introduction.html.

[2] N. a. Fleck, G. M. Muller, M. F. Ashby, and J. W. Hutchinson, "Strain gradient plasticity: Theory and experiment," *Acta Metall. Mater.*, vol. 42, no. 2, pp. 475–487, 1994.

[3] "BioMEMS and Microfluidics." [Online]. Available: http://biomems.eee.metu.edu.tr/biomems-and-microfludics/.

[4] R. Maranganti and P. Sharma, "Length Scales at which Classical Elasticity Breaks Down for Various Materials," *Phys. Rev. Lett.*, vol. 98, no. 19, p. 195504, 2007.

[5] M. Atkinson, "Further analysis of the size effect in indentation hardness tests of some metals," *J. Mater. Res.*, vol. 10, no. 11, pp. 2908–2915, 1995.

[6] Q. Ma and D. R. Clarke, "Size dependent hardness of silver single crystals," *J. Mater. Res.*, vol. 10, no. 4, pp. 853–863, 1995.

[7] W. J. Poole, M. F. Ashby, and N. a Fleck, "Micro-Hardness of Annealed and Work- Hardened Copper Polycrystals," *Acta Metall.*, vol. 34, no. 4, pp. 559–564, 1996.

[8] M. R. Begley and J. W. Hutchinson, "The mechanics of size-dependent indentation," *J. Mech. Phys. Solids*, vol. 46, no. 10, pp. 2049–2068, 1998.

[9] J. Y. Shu and N. a. Fleck, "The prediction of a size effect in microindentation," *Int. J. Solids Struct.*, vol. 35, no. 13, pp. 1363–1383, 1998.

[10] W. D. Nix and H. Gao, "Indentation size effects in crystalline materials: A law for strain gradient plasticity," *J. Mech. Phys. Solids*, vol. 46, no. 3, pp. 411–425, 1998.

[11] K. W. McElhaney, J. J. Vlassak, and W. D. Nix, “Determination of indenter tip geometry and indentation contact area for depth-sensing indentation experiments,” *J. Mater. Res.*, vol. 13, no. 5, pp. 1300–1306, 1998.

[12] Y. Yee Lim, M M Chaudhri, “The effect of the indenter load on the nanohardness of ductile metals: an experimental study on polycrystalline work-hardened and annealed oxygen-free copper,” *Philos. Mag. A*, vol. 79, no. 12, pp. 2979–3000, 1999.

[13] J. Swadener, “The correlation of the indentation size effect measured with indenters of various shapes,” *J. Mech. Phys. Solids*, vol. 50, no. 4, pp. 681–694, 2002.

[14] K. K. Tho, S. Swaddiwudhipong, J. Hua, and Z. S. Liu, “Numerical simulation of indentation with size effect,” *Mater. Sci. Eng. A*, vol. 421, no. 1–2, pp. 268–275, 2006.

[15] Y. Huang, F. Zhang, K. C. Hwang, W. D. Nix, G. M. Pharr, and G. Feng, “A model of size effects in nano-indentation,” *J. Mech. Phys. Solids*, vol. 54, no. 8, pp. 1668–1686, 2006.

[16] S. Qu, Y. Huang, G. M. Pharr, and K. C. Hwang, “The indentation size effect in the spherical indentation of iridium: A study via the conventional theory of mechanism-based strain gradient plasticity,” *Int. J. Plast.*, vol. 22, no. 7, pp. 1265–1286, 2006.

[17] E. Harsono, S. Swaddiwudhipong, Z. S. Liu, and L. Shen, “Numerical and experimental indentation tests considering size effects,” *Int. J. Solids Struct.*, vol. 48, no. 6, pp. 972–978, 2011.

[18] Y. Wei and J. W. Hutchinson, “Steady-state crack growth and work of fracture for solids characterized by strain gradient plasticity,” *J. Mech. Phys. Solids*, vol. 45, no. 8, pp. 1253–1273, 1997.

[19] J. S. Stölken and a. G. Evans, "A microbend test method for measuring the plasticity length scale," *Acta Mater.*, vol. 46, no. 14, pp. 5109–5115, 1998.

[20] P. Shrotriya, S. . Allameh, J. Lou, T. Buchheit, and W. . Soboyejo, "On the measurement of the plasticity length scale parameter in LIGA nickel foils," *Mech. Mater.*, vol. 35, no. 3–6, pp. 233–243, 2003.

[21] W. Wang, Y. Huang, K. J. Hsia, K. X. Hu, and a. Chandra, "A study of microbend test by strain gradient plasticity," *Int. J. Plast.*, vol. 19, no. 3, pp. 365–382, 2003.

[22] R. D. Mindlin and H. F. Tiersten, "Effects of couple-stresses in linear elasticity," *Arch. Ration. Mech. Anal.*, vol. 11, no. 1, pp. 415–448, 1962.

[23] R. Mindlin, "Micro-structure in linear elasticity," *Arch. Ration. Mech. Anal.*, 1964.

[24] R. D. Mindlin, "Second gradient of strain and surface-tension in linear elasticity," *Int. J. Solids Struct.*, vol. 1, no. 4, pp. 417–438, 1965.

[25] R. a. Toupin, "Elastic materials with couple-stresses," *Arch. Ration. Mech. Anal.*, vol. 11, no. 1, pp. 385–414, 1962.

[26] N. A. Fleck and J. W. Hutchinson, "a Phenomenological Theory for Strain Gradient Effects in Plasticity," *J. Mech. Phys. Solids*, 1993.

[27] N. Fleck and J. W. Hutchinson, "Strain Gradient Plasticity," *Advances in Applied Mechanics*, vol. 33. pp. 295–362, 1997.

[28] N. a. Fleck and J. W. Hutchinson, "A reformulation of strain gradient plasticity," *J. Mech. Phys. Solids*, vol. 49, no. 10, pp. 2245–2271, 2001.

[29] F. Yang, a. C. M. Chong, D. C. C. Lam, and P. Tong, "Couple stress based strain gradient theory for elasticity," *Int. J. Solids Struct.*, vol. 39, no. 10, pp. 2731–2743, 2002.

[30] D. C. C. Lam, F. Yang, a. C. M. Chong, J. Wang, and P. Tong, "Experiments and theory in strain gradient elasticity," *J. Mech. Phys. Solids*, vol. 51, no. 8, pp. 1477–

1508, 2003.

[31] a. C. Eringen, “On differential equations of nonlocal elasticity and solutions of screw dislocation and surface waves,” *J. Appl. Phys.*, vol. 54, no. 9, pp. 4703–4710, 1983.

[32] J. K. Phadikar and S. C. Pradhan, “Variational formulation and finite element analysis for nonlocal elastic nanobeams and nanoplates,” *Comput. Mater. Sci.*, vol. 49, no. 3, pp. 492–499, 2010.

[33] M. a. Eltaher, A. E. Alshorbagy, and F. F. Mahmoud, “Vibration analysis of Euler–Bernoulli nanobeams by using finite element method,” *Appl. Math. Model.*, vol. 37, pp. 4787–4797, 2012.

[34] F. F. Mahmoud, M. a. Eltaher, a. E. Alshorbagy, and E. I. Meletis, “Static analysis of nanobeams including surface effects by nonlocal finite element,” *J. Mech. Sci. Technol.*, vol. 26, no. 11, pp. 3555–3563, 2012.

[35] M. a. Eltaher, S. a. Emam, and F. F. Mahmoud, “Static and stability analysis of nonlocal functionally graded nanobeams,” *Compos. Struct.*, vol. 96, pp. 82–88, 2013.

[36] J. N. Reddy and S. El-Borgi, “Eringen’s nonlocal theories of beams accounting for moderate rotations,” *Int. J. Eng. Sci.*, vol. 82, pp. 159–177, 2014.

[37] J. N. Reddy, S. El-Borgi, and J. Romanoff, “Non-linear analysis of functionally graded microbeams using Eringens non-local differential model,” *Int. J. Non. Linear. Mech.*, vol. 67, pp. 308–318, 2014.

[38] S. C. Pradhan, “Nonlocal finite element analysis and small scale effects of CNTs with Timoshenko beam theory,” *Finite Elem. Anal. Des.*, vol. 50, pp. 8–20, 2012.

[39] A. a. Pisano, A. Sofi, and P. Fuschi, “Finite element solutions for nonhomogeneous nonlocal elastic problems,” *Mech. Res. Commun.*, vol. 36, no. 7, pp. 755–761, 2009.

[40] S. Natarajan, S. Chakraborty, M. Thangavel, S. Bordas, and T. Rabczuk, "Size-dependent free flexural vibration behavior of functionally graded nanoplates," *Comput. Mater. Sci.*, vol. 65, pp. 74–80, 2012.

[41] Ö. Civalek and Ç. Demir, "Bending analysis of microtubules using nonlocal Euler-Bernoulli beam theory," *Appl. Math. Model.*, vol. 35, no. 5, pp. 2053–2067, 2011.

[42] M. Z. Nejad and A. Hadi, "Non-local analysis of free vibration of bi-directional functionally graded Euler-Bernoulli nano-beams," *Int. J. Eng. Sci.*, vol. 105, pp. 1–11, 2016.

[43] M. Z. Nejad, A. Hadi, and A. Rastgoo, "Buckling analysis of arbitrary two-directional functionally graded Euler-Bernoulli nano-beams based on nonlocal elasticity theory," *Int. J. Eng. Sci.*, vol. 103, pp. 1–10, 2016.

[44] M. Z. Nejad and A. Hadi, "Eringen's non-local elasticity theory for bending analysis of bi-directional functionally graded Euler-Bernoulli nano-beams," *Int. J. Eng. Sci.*, vol. 106, pp. 1–9, 2016.

[45] M. Ghadiri and N. Shafiei, "Nonlinear bending vibration of a rotating nanobeam based on nonlocal Eringen???s theory using differential quadrature method," *Microsyst. Technol.*, vol. 22, no. 12, pp. 2853–2867, 2016.

[46] N. Shafiei, M. Kazemi, M. Safi, and M. Ghadiri, "Nonlinear vibration of axially functionally graded non-uniform nanobeams," *Int. J. Eng. Sci.*, vol. 106, pp. 77–94, 2016.

[47] A. Daneshmehr, A. Rajabpoor, and M. Pourdavood, "Stability of size dependent functionally graded nanoplate based on nonlocal elasticity and higher order plate theories and different boundary conditions," *Int. J. Eng. Sci.*, vol. 82, pp. 84–100, 2014.

[48] A. Daneshmehr, A. Rajabpoor, and A. Hadi, "Size dependent free vibration

analysis of nanoplates made of functionally graded materials based on nonlocal elasticity theory with high order theories," *Int. J. Eng. Sci.*, vol. 95, pp. 23–35, 2015.

[49] J. N. Reddy, "Nonlocal theories for bending, buckling and vibration of beams," *Int. J. Eng. Sci.*, vol. 45, no. 2–8, pp. 288–307, 2007.

[50] M. Aydogdu, "A general nonlocal beam theory: Its application to nanobeam bending, buckling and vibration," *Phys. E Low-Dimensional Syst. Nanostructures*, vol. 41, no. 9, pp. 1651–1655, 2009.

[51] J. C. Hsu, H. L. Lee, and W. J. Chang, "Longitudinal vibration of cracked nanobeams using nonlocal elasticity theory," *Curr. Appl. Phys.*, vol. 11, no. 6, pp. 1384–1388, 2011.

[52] T. Murmu and S. Adhikari, "Nonlocal elasticity based vibration of initially pre-stressed coupled nanobeam systems," *Eur. J. Mech. A/Solids*, vol. 34, pp. 52–62, 2012.

[53] M. Şimşek and H. H. Yurtcu, "Analytical solutions for bending and buckling of functionally graded nanobeams based on the nonlocal Timoshenko beam theory," *Compos. Struct.*, vol. 97, pp. 378–386, 2013.

[54] B. Uymaz, "Forced vibration analysis of functionally graded beams using nonlocal elasticity," *Composite Structures*, vol. 105. Elsevier Ltd, pp. 227–239, 2013.

[55] O. Rahmani and O. Pedram, "Analysis and modeling the size effect on vibration of functionally graded nanobeams based on nonlocal Timoshenko beam theory," *Int. J. Eng. Sci.*, vol. 77, pp. 55–70, 2014.

[56] R. Nazemnezhad and S. Hosseini-Hashemi, "Nonlocal nonlinear free vibration of functionally graded nanobeams," *Compos. Struct.*, vol. 110, no. 1, pp. 192–199, 2014.

[57] M. Tuna and M. Kirca, “Exact solution of Eringen’s nonlocal integral model for bending of Euler-Bernoulli and Timoshenko beams,” *Int. J. Eng. Sci.*, vol. 105, pp. 80–92, 2016.

[58] J. Fernandez-Saez, R. Zaera, J. A. Loya, and J. N. Reddy, “Bending of Euler-Bernoulli beams using Eringen’s integral formulation: A paradox resolved,” *Int. J. Eng. Sci.*, vol. 99, pp. 107–116, 2016.

[59] H. Salehipour, A. R. Shahidi, and H. Nahvi, “Modified nonlocal elasticity theory for functionally graded materials,” *Int. J. Eng. Sci.*, vol. 90, pp. 44–57, 2015.

[60] P. Khodabakhshi and J. N. Reddy, “A unified integro-differential nonlocal model,” *Int. J. Eng. Sci.*, vol. 95, pp. 60–75, 2015.

[61] S. Kong, S. Zhou, Z. Nie, and K. Wang, “Static and dynamic analysis of micro beams based on strain gradient elasticity theory,” *Int. J. Eng. Sci.*, vol. 47, no. 4, pp. 487–498, 2009.

[62] B. Wang, J. Zhao, and S. Zhou, “A micro scale Timoshenko beam model based on strain gradient elasticity theory,” *Eur. J. Mech. A/Solids*, vol. 29, no. 4, pp. 591–599, 2010.

[63] M. H. Kahrobaiyan, M. Asghari, M. Rahaeifard, and M. T. Ahmadian, “A nonlinear strain gradient beam formulation,” *Int. J. Eng. Sci.*, vol. 49, no. 11, pp. 1256–1267, 2011.

[64] M. H. Kahrobaiyan, M. Rahaeifard, S. a. Tajalli, and M. T. Ahmadian, “A strain gradient functionally graded Euler-Bernoulli beam formulation,” *Int. J. Eng. Sci.*, vol. 52, pp. 65–76, 2012.

[65] B. Akgöz and Ö. Civalek, “Application of strain gradient elasticity theory for buckling analysis of protein microtubules,” *Curr. Appl. Phys.*, vol. 11, no. 5, pp. 1133–1138, 2011.

[66] B. Akgöz and Ö. Civalek, “A new trigonometric beam model for buckling of strain

gradient microbeams," *Int. J. Mech. Sci.*, vol. 81, pp. 88–94, 2014.

[67] B. Akgöz and Ö. Civalek, "Shear deformation beam models for functionally graded microbeams with new shear correction factors," *Compos. Struct.*, vol. 112, pp. 214–225, 2014.

[68] R. Aghazadeh, "Static And Free Vibration Analyses Of Small - Scale Functıonally Graded Beams Possessing A Variable Length Scale Parameter Using Different Beam Theories," Middle East Technical University, 2013.

[69] B. Zhang, Y. He, D. Liu, Z. Gan, and L. Shen, "Non-classical Timoshenko beam element based on the strain gradient elasticity theory," *Finite Elem. Anal. Des.*, vol. 79, pp. 22–39, 2014.

[70] M. Hosseini and R. Bahaadini, "Size dependent stability analysis of cantilever micro-pipes conveying fluid based on modified strain gradient theory," *Int. J. Eng. Sci.*, vol. 101, pp. 1–13, Apr. 2016.

[71] H. Dal, "Analysis of Gold Micro-Beams with Modified Strain Gradient Theory," *Anadolu Univ. J. Sci. Technol.*, pp. 663–681, 2017.

[72] S. K. Park and X.-L. Gao, "Bernoulli–Euler beam model based on a modified couple stress theory," *J. Micromechanics Microengineering*, vol. 16, no. 11, pp. 2355–2359, 2006.

[73] S. Kong, S. Zhou, Z. Nie, and K. Wang, "The size-dependent natural frequency of Bernoulli-Euler micro-beams," *Int. J. Eng. Sci.*, vol. 46, no. 5, pp. 427–437, 2008.

[74] W. Xia, L. Wang, and L. Yin, "Nonlinear non-classical microscale beams: Static bending, postbuckling and free vibration," *Int. J. Eng. Sci.*, vol. 48, no. 12, pp. 2044–2053, 2010.

[75] S. K. Park and X. L. Gao, "Variational formulation of a modified couple stress theory and its application to a simple shear problem," *Zeitschrift fur Angew. Math.*

und Phys., vol. 59, no. 5, pp. 904–917, 2008.

[76] M. Asghari, M. T. Ahmadian, M. H. Kahrobaiyan, and M. Rahaeifard, "On the size-dependent behavior of functionally graded micro-beams," *Mater. Des.*, vol. 31, no. 5, pp. 2324–2329, 2010.

[77] M. Asghari, M. Rahaeifard, M. H. Kahrobaiyan, and M. T. Ahmadian, "The modified couple stress functionally graded Timoshenko beam formulation," *Mater. Des.*, vol. 32, no. 3, pp. 1435–1443, 2011.

[78] J. N. Reddy, "Microstructure-dependent couple stress theories of functionally graded beams," *J. Mech. Phys. Solids*, vol. 59, no. 11, pp. 2382–2399, 2011.

[79] Y. Fu and J. Zhang, "Modeling and analysis of microtubules based on a modified couple stress theory," *Phys. E Low-Dimensional Syst. Nanostructures*, vol. 42, no. 5, pp. 1741–1745, 2010.

[80] H. M. Ma, X. L. Gao, and J. N. Reddy, "A microstructure-dependent Timoshenko beam model based on a modified couple stress theory," *J. Mech. Phys. Solids*, vol. 56, no. 12, pp. 3379–3391, 2008.

[81] B. Akgöz and Ö. Civalek, "Strain gradient elasticity and modified couple stress models for buckling analysis of axially loaded micro-scaled beams," *Int. J. Eng. Sci.*, vol. 49, no. 11, pp. 1268–1280, 2011.

[82] B. Akgöz and Ö. Civalek, "Stability Analysis of Carbon Nanotubes (CNTs) Based on Modified Couple Stress Theory," vol. 2, no. May, pp. 16–18, 2011.

[83] M. M. S. Fakhrabadi, A. Rastgoo, M. T. Ahmadian, and M. M. Mashhadi, "Dynamic analysis of carbon nanotubes under electrostatic actuation using modified couple stress theory," *Acta Mech.*, vol. 1535, pp. 1523–1535, 2013.

[84] M. Şimşek, "Nonlinear static and free vibration analysis of microbeams based on the nonlinear elastic foundation using modified couple stress theory and He's variational method," *Compos. Struct.*, vol. 112, pp. 264–272, 2014.

[85] M. H. Ghayesh and H. Farokhi, "Chaotic motion of a parametrically excited microbeam," *Int. J. Eng. Sci.*, vol. 96, pp. 34–45, 2015.

[86] M. Rahaeifard, "Static behavior of bilayer microcantilevers under thermal actuation," *Int. J. Eng. Sci.*, vol. 107, pp. 28–35, 2016.

[87] R. Sourki and S. A. H. Hoseini, "Free vibration analysis of size-dependent cracked microbeam based on the modified couple stress theory," *Appl. Phys. A Mater. Sci. Process.*, vol. 122, no. 4, pp. 1–11, 2016.

[88] M. Mohammad Abadi and a. R. Daneshmehr, "An investigation of modified couple stress theory in buckling analysis of micro composite laminated Euler-Bernoulli and Timoshenko beams," *Int. J. Eng. Sci.*, vol. 75, pp. 40–53, 2014.

[89] H. T. Thai, T. P. Vo, T. K. Nguyen, and J. Lee, "Size-dependent behavior of functionally graded sandwich microbeams based on the modified couple stress theory," *Compos. Struct.*, vol. 123, pp. 337–349, 2015.

[90] M. R. Ilkhani and S. H. Hosseini-Hashemi, "Size dependent vibro-buckling of rotating beam based on modified couple stress theory," *Compos. Struct.*, vol. 143, pp. 75–83, 2016.

[91] M. Şimşek and J. N. Reddy, "Bending and vibration of functionally graded microbeams using a new higher order beam theory and the modified couple stress theory," *Int. J. Eng. Sci.*, vol. 64, pp. 37–53, 2013.

[92] J. Lei, Y. He, B. Zhang, D. Liu, L. Shen, and S. Guo, "A size-dependent FG micro-plate model incorporating higher-order shear and normal deformation effects based on a modified couple stress theory," *Int. J. Mech. Sci.*, vol. 104, pp. 8–23, 2015.

[93] J. Lou, L. He, and J. Du, "A unified higher order plate theory for functionally graded microplates based on the modified couple stress theory," *Compos. Struct.*, vol. 133, pp. 1036–1047, 2015.

[94] E. Taati, “Analytical solutions for the size dependent buckling and postbuckling behavior of functionally graded micro-plates,” *Int. J. Eng. Sci.*, vol. 100, pp. 45–60, 2016.

[95] J. Guo, J. Chen, and E. Pan, “Size-dependent behavior of functionally graded anisotropic composite plates,” *Int. J. Eng. Sci.*, vol. 106, pp. 110–124, 2016.

[96] J. Lou, L. He, J. Du, and H. Wu, “Nonlinear analyses of functionally graded microplates based on a general four-variable refined plate model and the modified couple stress theory,” *Compos. Struct.*, vol. 152, pp. 516–527, 2016.

[97] L. Wang, “Size-dependent vibration characteristics of fluid-conveying microtubes,” *J. Fluids Struct.*, vol. 26, no. 4, pp. 675–684, 2010.

[98] L. L. Ke, Y. S. Wang, J. Yang, and S. Kitipornchai, “Nonlinear free vibration of size-dependent functionally graded microbeams,” *Int. J. Eng. Sci.*, vol. 50, no. 1, pp. 256–267, 2012.

[99] N. Shafiei, M. Kazemi, and M. Ghadiri, “On size-dependent vibration of rotary axially functionally graded microbeam,” *Int. J. Eng. Sci.*, vol. 101, pp. 29–44, 2016.

[100] N. Shafiei, A. Mousavi, and M. Ghadiri, “On size-dependent nonlinear vibration of porous and imperfect functionally graded tapered microbeams,” *Int. J. Eng. Sci.*, vol. 106, pp. 42–56, 2016.

[101] N. Shafiei, M. Kazemi, and M. Ghadiri, “Nonlinear vibration of axially functionally graded tapered microbeams,” *Int. J. Eng. Sci.*, vol. 102, pp. 12–26, 2016.

[102] M. Mohammad-Abadi and a. R. Daneshmehr, “Size dependent buckling analysis of microbeams based on modified couple stress theory with high order theories and general boundary conditions,” *Int. J. Eng. Sci.*, vol. 74, pp. 1–14, 2014.

[103] M. Akbarzadeh Khorshidi, M. Shariati, and S. A. Emam, “Postbuckling of

functionally graded nanobeams based on modified couple stress theory under general beam theory," *Int. J. Mech. Sci.*, vol. 110, pp. 160–169, 2016.

[104] A. Arbind and J. N. Reddy, "Nonlinear analysis of functionally graded microstructure-dependent beams," *Compos. Struct.*, vol. 98, pp. 272–281, 2013.

[105] M. H. Kahrobaiyan, M. Asghari, and M. T. Ahmadian, "A Timoshenko beam element based on the modified couple stress theory," *Int. J. Mech. Sci.*, vol. 79, pp. 75–83, 2014.

[106] H. L. Dai, Y. K. Wang, and L. Wang, "Nonlinear dynamics of cantilevered microbeams based on modified couple stress theory," *Int. J. Eng. Sci.*, vol. 94, pp. 103–112, 2015.

[107] A. M. Dehrouyeh-Semnani, "The influence of size effect on flapwise vibration of rotating microbeams," *Int. J. Eng. Sci.*, vol. 94, pp. 150–163, 2015.

[108] A. M. Dehrouyeh-Semnani and M. Nikkhah-Bahrami, "The influence of size-dependent shear deformation on mechanical behavior of microstructures-dependent beam based on modified couple stress theory," *Compos. Struct.*, vol. 123, pp. 325–336, 2015.

[109] A. M. Dehrouyeh-Semnani, M. BehboodiJouybari, and M. Dehrouyeh, "On size-dependent lead-lag vibration of rotating microcantilevers," *Int. J. Eng. Sci.*, vol. 101, pp. 50–63, 2016.

[110] A. M. Dehrouyeh-Semnani and A. Behrami, "On size-dependent Timoshenko beam element based on modified couple stress theory," *Int. J. Eng. Sci.*, vol. 51, pp. 292–309, 2016.

[111] J. N. Reddy, J. Romanoff, and J. A. Loya, "Nonlinear finite element analysis of functionally graded circular plates with modified couple stress theory," *Eur. J. Mech. - A/Solids*, vol. 56, pp. 92–104, 2016.

[112] F. B. Hildebrand, *Methods of Applied Mathematics*, Second. New Jersey:

Prentice-Hall, INC., 1952.

[113] J. N. Reddy, *J.N. Reddy An Introduction to the Finite Element Method, 3rd Edition 2005.pdf*, Third. Texas: McGraw Hill, 2005.

[114] G. R. Liu and S. S. Quek, *The Finite Element Method A Practical Course*,1st edition 2003, Jordan Hill, Oxford, Burlington.,2003.

[115] J. Lin and R. G. Parker, "Mesh Stiffness Variation Instabilities in Two-Stage Gear Systems," *J. Vib. Acoust.*, vol. 124, no. 1, p. 68, 2002.

[116] J. Lin and R. G. Parker, "Planetary gear parametric instability caused by mesh stiffness variation," *J. Sound Vib.*, vol. 249, no. 1, pp. 129–145, 2002.

[117] L. Yinong, L. Guiyan, and Z. Ling, "Influence of asymmetric mesh stiffness on dynamics of spiral bevel gear transmission system," *Math. Probl. Eng.*, vol. 2010, 2010.

[118] T. D. Mathur, E. C. Smith, H. Desmidt, and R. C. Bill, "Load Distribution and Mesh Stiffness Analysis of an Internal-External Bevel Gear Pair in a Pericyclic Drive," *AHS 72nd Annu. Foru*, 2016.

[119] L. Chang, G. Liu, and L. Wu, "A robust model for determining the mesh stiffness of cylindrical gears," *MAMT*, vol. 87, pp. 93–114, 2015.

[120] D. B. Dooner, *Kinematic Geometry of Gearing*, 2nd ed. John Wiley & Sons, Ltd., Publication, 2012.

[121] J. J. Sniegowski and E. J. Garcia, "Surface-micromachined gear trains driven by an on-chip electrostatic microengine," *IEEE Electron Device Lett.*, vol. 17, no. 7, pp. 366–368, 1996.

[122] F. L. Litvin and A. Fuentes, *Gear Geometry And Applied Theory*, 2nd ed. New York: Cambrdige University Press, 2004.

[123] A. Beheshti, "Finite element analysis of plane strain solids in strain-gradient elasticity," *Acta Mech.*, vol. 228, no. 10, pp. 3543–3559, 2017.

[124] M. Peng and H. A. DeSmidt, “Torsional Stability of a Face-Gear Drive System,” *AHS 68th Annu. Forum*, 2012.

[125] I. Standard, “ISO 6336-1,” vol. 1, 2007.

APPENDIX A

CODE FOR BEAM STRUCTURE

Main Body of the Code

```
format long
clear all
% Properties of Beam
E=1440; l=17.6*10^-3; h=35.2*10^-3; b=h; A=b*h; I=(1/12)*b*h^3;
EA=E*A; EI=E*I; nu=0.38; mu=E/(2*(1+nu)); a=(mu*A*l^2)/(E*I);
ro=1.22*10^-9;
% generation of coordinates and connectivities
numberElements=12;
nodeCoordinates=[0 0;0 0.088;0 0.176;0 0.264;
0 0.352;0.088 0.352;0.176 0.352;
0.264 0.352;0.352 0.352;0.352 0.264;
0.352 0.176;0.352 0.088;0.352 0];
xx=nodeCoordinates;
for i=1:numberElements;
elementNodes(i,1)=i;
elementNodes(i,2)=i+1;
end
numberNodes=size(nodeCoordinates,1);
xx=nodeCoordinates(:,1);
```

```
yy=nodeCoordinates(:,2);
GDof=3*numberNodes; % global number of degrees of freedom
U=zeros(GDof,1);
force=zeros(GDof,1);
stiffness=zeros(GDof);
%force vector
force(5)=0.001;
% stiffness matrix
[stiffness]=MicroformStiffness2Dframe(GDof,numberElements,elementNodes,number
Nodes,xx,yy,EI,EA,a);
% mass matrix
[mass]=Microformmass2Dframe(GDof,numberElements,elementNodes,numberNodes,
xx,yy,ro,I,A);
%% boundary conditions
prescribedDo=[1 13 14 26 27 39];
prescribedDof=transpose(prescribedDo);
%% solution
% Deflections
displacements=Microsolution(GDof,prescribedDof,stiffness,force)
% Frequencies
activeDof=setdiff((1:GDof),(prescribedDof));
[vec1,d1]=eig(mass(activeDof,activeDof)^-1*stiffness(activeDof,activeDof));
[d1,In1]=sort(abs(diag(d1)));
vec1=real(vec1(:,In1));
wn1=sqrt(d1);
Khertz1=wn1/(2*pi)/1000
```

Stiffness Matrices function:

```
function
[stiffness]=MicroformStiffness2Dframe(GDof,numberElements,elementNodes,number
Nodes,xx,yy,EI,EA,a)
stiffness=zeros(GDof);
% computation of the system stiffness matrix
for e=1:numberElements;
indice=elementNodes(e,:) ;
elementDof=[ indice indice+numberNodes indice+2*numberNodes] ;
nn=length(indice);
xa=xx(indice(2))-xx(indice(1));
ya=yy(indice(2))-yy(indice(1));
length_element=sqrt(xa*xa+ya*ya);
cosa=xa/length_element;
sena=ya/length_element;
ll=length_element;
L= [cosa*eye(2) sena*eye(2) zeros(2);
-sena*eye(2) cosa*eye(2) zeros(2);
zeros(2,4) eye(2)];
oneu=[1 -1;-1 1];
oneu2=[1 -1;1 -1];
oneu3=[1 1;-1 -1];
oneu4=[4 2;2 4];
k1=[EA/ll*oneu zeros(2,4);
zeros(2) 12*(1+a)*EI/ll^3*oneu 6*(1+a)*EI/ll^2*oneu3;
zeros(2) 6*(1+a)*EI/ll^2*oneu2 EI*(1+a)/ll*oneu4];
stiffness(elementDof,elementDof)=stiffness(elementDof,elementDof)+L^-1*k1*L;
end
```

Mass Matrices function:

```
function
[mass]=Microformmass2Dframe(GDof,numberElements,elementNodes,numberNodes,
xx,yy,ro,I,A)
mass=zeros(GDof);
%% Element Mass Matrix
for e=1:numberElements;
% elementDof: element degrees of freedom (Dof)
indice=elementNodes(e,:) ;
elementDof=[ indice indice+numberNodes indice+2*numberNodes] ;
nn=length(indice);
xa=xx(indice(2))-xx(indice(1));
ya=yy(indice(2))-yy(indice(1));
length_element=sqrt(xa*xa+ya*ya);
cosa=xa/length_element;
sena=ya/length_element;
ll=length_element;
roAL=ro*A*ll;
roI=ro*I;
L= [cosa*eye(2) sena*eye(2) zeros(2);
-sena*eye(2) cosa*eye(2) zeros(2);
zeros(2,4) eye(2)];
oneuu=[140 70;70 140];
oneu=[156 54;54 156];
oneu2=[22 13;-13 -22];
oneu3=[22 -13;13 -22];
```

```
oneu4=[4 -3;-3 4];
oneux=[36 -36;-36 36];
oneu3x=[3 3;-3 -3];
oneu2x=[3 -3;3 -3];
oneu4x=[4 -1;1 4];
k1x=[(roAL/420)*oneuu zeros(2,4);
zeros(2) (roAL/420)*oneu (roAL/420)*ll*oneu3;
zeros(2) (roAL/420)*ll*oneu2 (roAL/420)*ll^2*oneu4];
k2x=[0*oneuu zeros(2,4);
zeros(2) (roI/(30*ll))*oneux (roI/(30*ll))*ll*oneu3x;
zeros(2) (roI/(30*ll))*ll*oneu2x (roI/(30*ll))*ll^2*oneu4x];
k1=k1x+k2x;
mass(elementDof,elementDof)=mass(elementDof,elementDof)+L^-1*k1*L;
end
```

Solution:

```
function displacements=Microsolution(GDof,prescribedDof,stiffness,force)
% function to find solution in terms of global displacements
activeDof=setdiff((1:GDof),(prescribedDof));
U=stiffness(activeDof,activeDof)\force(activeDof);
% U=stiffness(activeDof,activeDof)\force(activeDof);
displacements=zeros(GDof,1);
displacements(activeDof)=U;
```